

Yet Another Tensor Toolbox for discontinuous Galerkin methods and other applications

CARSTEN UPHOFF, Technical University of Munich, Germany

MICHAEL BADER, Technical University of Munich, Germany

The numerical solution of partial differential equations is at the heart of many grand challenges in supercomputing. Solvers based on high-order discontinuous Galerkin (DG) discretisation have been shown to scale on large supercomputers with excellent performance and efficiency, if the implementation exploits all levels of parallelism and is tailored to the specific architecture. However, every year new supercomputers emerge and the list of hardware-specific considerations grows, simultaneously with the list of desired features in a DG code. Thus we believe that a sustainable DG code needs an abstraction layer to implement the numerical scheme in a suitable language. We explore the possibility to abstract the numerical scheme as small tensor operations, describe them in a domain-specific language (DSL) resembling the Einstein notation, and to map them to existing code generators which generate small matrix matrix multiplication routines. The compiler for our DSL implements classic optimisations that are used for large tensor contractions, and we present novel optimisation techniques such as equivalent sparsity patterns and optimal index permutations for temporary tensors. Our application examples, which include the earthquake simulation software SeisSol, show that the generated kernels achieve over 50 % peak performance while the DSL considerably simplifies the implementation.

CCS Concepts: • **Computing methodologies** → **Massively parallel and high-performance simulations**; • **Software and its engineering** → **Source code generation**; **Domain specific languages**; • **Applied computing** → **Earth and atmospheric sciences**;

ACM Reference Format:

Carsten Uphoff and Michael Bader. 2019. Yet Another Tensor Toolbox for discontinuous Galerkin methods and other applications. *ACM Trans. Math. Softw.* 1, 1 (March 2019), 32 pages. <https://doi.org/0000001.0000001>

1 INTRODUCTION

Solving partial differential equations (PDEs) is one of the pillars of computational science and engineering, and solving PDEs accurately on a computer is one of the grand challenges in high performance computing. Simulations may have billions of degrees of freedom, hence highly scalable codes that make efficient use of the invested energy are required. But, highly efficient software often requires expert knowledge, the resulting code might not reflect the underlying numerical scheme, and code tends to become complex: While on the one hand a software might want to support several PDEs, several finite element types, or multi-physics simulations, on the other hand developers have to deal with the subtleties of modern hardware architectures, for example vector instruction latency or level 1 cache bandwidth. Moreover, evolution of hardware architectures may require the adaption of all implemented combinations or even a radical change of data structures.

Authors' addresses: Carsten Uphoff, Technical University of Munich, Boltzmannstr. 3, 85748, Garching, Germany, uphoff@in.tum.de; Michael Bader, Technical University of Munich, Boltzmannstr. 3, 85748, Garching, Germany, bader@in.tum.de.

Permission to make digital or hard copies of all or part of this work for personal or classroom use is granted without fee provided that copies are not made or distributed for profit or commercial advantage and that copies bear this notice and the full citation on the first page. Copyrights for components of this work owned by others than the author(s) must be honored. Abstracting with credit is permitted. To copy otherwise, or republish, to post on servers or to redistribute to lists, requires prior specific permission and/or a fee. Request permissions from permissions@acm.org.

© 2019 Copyright held by the owner/author(s). Publication rights licensed to ACM.

Manuscript submitted to ACM

Manuscript submitted to ACM

1

A strategy to deal with the mentioned complexity is to choose a proper abstraction. For example in linear algebra, a lot of operations may be implemented with only a few simple inner-most kernels (e.g. [Van Zee and van de Geijn 2015]). The advantage is two-fold, as firstly only a few kernels need to be optimised by an expert, and secondly all projects that build up on these kernels may benefit from improvements. Abstracting algorithms in terms of linear algebra operations, especially the General Matrix-Matrix Multiplication (GEMM), is becoming popular for the numerical solution of PDEs, too. High-order discontinuous Galerkin (DG) or spectral element methods usually consist of small element local operators, such that its implementations may be expressed as sequence of small GEMMs [Breuer et al. 2017; Hutchinson et al. 2016; Uphoff et al. 2017; Vincent et al. 2016]. The matrices are usually small enough, such that data movement considerations within a GEMM become irrelevant. At the same time, the overhead of calling BLAS and the choice of GEMM micro-kernels becomes significant, such that specialised code generators for small GEMMs are employed [Heinecke et al. 2016b], or even specialised code generators for small tensor contractions are developed [Breuer et al. 2017]. An alternative ansatz is to express tensor operations in an appropriate intermediate representation, which captures the underlying loop structure, and use compiler techniques and cost models in order to generate efficient code [Kempf et al. 2018; Luporini et al. 2015; Stock et al. 2011].

The abstraction of tensor operations is not new but has been researched for decades in the field of computational chemistry. Here, one may distinguish two different levels of abstraction: The first level of abstraction is the move from an expression involving several tensors to binary tensor operations. On this level of abstraction, algebraic transformations may be employed. In the so-called strength reduction, for example, the optimal sequence of tensor operations is determined (under a memory constraint) such that the total number of floating point operations is minimised, which is then usually magnitudes smaller than a naive implementation [Lam et al. 1997]. The most prominent representative is the Tensor Contraction Engine (TCE) [Baumgartner et al. 2005], but also a framework called Barracuda for GPUs exists [Nelson et al. 2015]. The second level of abstraction is the implementation of binary tensor operations, especially for tensor contractions. For the latter, a variety of algorithms exist, such as nested-loop code, Loop-over-GEMMs (LoG), Transpose-Transpose-GEMM-Transpose (TTGT), and GEMM-like Tensor-Tensor multiplication (GETT) [Springer and Bientinesi 2018, and references therein].

In computational chemistry tensors may become very large, such that intermediate results may not remain in memory but must be loaded from disk [Baumgartner et al. 2005]. So despite the fact that quantum chemistry models and high-order DG methods may be abstracted as tensor operations, the situation is quite different for the latter, as shall be outlined in the following:

- All matrices fit inside memory or even inside low-level caches. There is no need to optimise for memory usage or fuse loops to trade off memory usage and operation count [Baumgartner et al. 2005].
- Tensor operations do not need to be distributed among nodes.
- Data copies or index permutations may be amortised for large GEMMs [Goto and van de Geijn 2008; Springer and Bientinesi 2018], as these scale with $O(N^2)$ compared to $O(N^3)$, but this is usually not the case for small GEMMs [Heinecke et al. 2016b]. (Which excludes TTGT.)
- All tensor dimensions and respective sparsity patterns in element-local operations are known a priori. Furthermore, spending a lot of time optimising individual tensor operations can be justified, as those are called millions of times during simulations [Uphoff et al. 2017].
- Sparsity can be dealt with explicitly, as it is feasible to compute the sparsity pattern of a tensor operation during the invocation of a code generator. There is no need to estimate the sparsity, as proposed in [Lam 1999].

- Some optimisations are special to small GEMMs or DG methods, such as padding matrices for optimal vectorisation or tailored software prefetching schemes [Heinecke et al. 2016a].

Other publications and open-source packages focus on binary tensor contractions [Li et al. 2015; Matthews 2018; Shi et al. 2016; Solomonik et al. 2013; Springer and Bientinesi 2018], GPUs [Nelson et al. 2015], or focus on loop transformations [Kempf et al. 2018; Luporini et al. 2015; Stock et al. 2011], where the latter lack support for sparse matrices in element-local operators and are to our understanding not designed for use with code generators for small GEMMs.

We therefore present **Yet Another Tensor Toolbox** (YATeTo), which we explicitly designed for the use in PDE solvers. In YATeTo, tensor operations are described in a high-level language that is motivated by the Einstein convention. An abstract syntax tree (AST) is formed on which algebraic transformations and other optimisations are done. Afterwards, code generators for small GEMMs are called and finally C++-code is generated which calls either generated code or calls BLAS libraries. Our design does not prescribe the use of a specific implementation of binary tensor contractions, but allows to choose the implementation based on operation type and hardware architecture. Note that our main focus are high-order DG and spectral element methods, and that our ultimate goal is that the performance of the YATeTo-generated code matches the performance of hand-crafted code, but the toolbox itself may be used for arbitrary applications where small tensor operations are required and tensor dimensions and respective sparsity patterns are known a priori.

2 RELATED WORK

Many components of YATeTo build on previous algorithms and ideas. In this section we summarise related work and necessary background.

2.1 High-level language and representation

The need for high-level languages for tensor contractions was already clear to A. Einstein, who wrote in the foundations of general relativity:

“Dafür führen wir die Vorschrift ein: Tritt ein Index in einem Term eines Ausdrucks zweimal auf, so ist über ihn stets zu summieren, wenn nicht ausdrücklich das Gegenteil bemerkt ist.” [Einstein 1916]

The so-called Einstein convention states that one shall sum over every index that appears twice in a term. Elegant domain-specific languages may be defined using this convention. For example, in the Cyclops tensor framework one may write [Solomonik et al. 2013]

```
W["MnIj"] = V["MnEf"] * T["EfIj"];
Z["AbIj"] = W["MnIj"] * T["AbMn"];
```

which is valid C++ (using operator overloading) and implements

$$z_{abij} = \sum_{mn} t_{abmn} \left(\sum_{ef} v_{mnef} t_{efij} \right).$$

The Barracuda framework defines a similar high-level language [Nelson et al. 2015].

In the TCE, tensor operations are represented internally as function sequences consisting of two types of formulae [Lam et al. 1997]: The first type is a multiplication formula of the form $f_r[\dots] = X[\dots] \times Y[\dots]$. Depending on the indices inside the square brackets a different operation is represented. E.g. $f_r[i, j] = X[i] \times Y[j]$ represents a tensor

product whereas $f_r[i] = X[i] \times Y[i]$ represents a Hadamard product. (Note that two indices appear but are not summed over, that is, this representation does not adhere to the Einstein convention.) The second type is a summation formula of the form $f_r[\dots] = \sum_i X[\dots]$. Here, the dimension of the left-hand side is always one less than the right-hand side, and the dimension to be summed over is determined by the indices in the brackets.

2.2 Strength reduction

In many cases there are many mathematically equivalent ways to implement tensor operations. In [Baumgartner et al. 2005] the following motivating example is given, where each dimension has size N ,

$$S_{abij} = \sum_{cdefkl} A_{acik} B_{befl} C_{dfjk} D_{cdel} = \sum_{ck} \left(\sum_{df} \left(\sum_{el} B_{befl} D_{cdel} \right) C_{dfjk} \right) A_{acik}$$

The first implementation corresponds to the naive implementation with 10 nested loops, which requires $4N^{10}$ operations. The second implementation saves intermediate results and only requires $6N^6$ operations. Hence, the second implementation is four orders of magnitudes cheaper than the first implementation.

Naturally, one asks if and how optimal implementations can be found automatically. A formal optimisation problem is set up in [Lam et al. 1997] using the two types of formulae mentioned in Section 2.1. It is shown that this optimisation problem is NP-complete and an efficient search procedure is developed in [Lam et al. 1997], which exhaustively searches all valid formulae and hence finds the optimal implementation. As the number of dimensions arising in practice is typically small, this search procedure is feasible. The number of dimensions is also small enough in our application examples, see Section 5, hence there is no need to develop new algorithms for strength reduction.

2.3 Loop-over-GEMM (LoG)

The authors of [Di Napoli et al. 2014] give a summary of tensor contraction classes and possible mappings to BLAS. In a binary contraction, the contraction is classified in the number of free indices of each input tensor. (That is, those indices which are not contracted.) The most interesting case is when both tensors have at least one free index, as in this case a mapping to GEMM is always possible, if data is allowed to be copied or non-stride-one-GEMMs are considered.

Consider the following contraction from [Springer and Bientinesi 2018]:

$$C_{abcijk} := \sum_m A_{ijmc} B_{mkab}.$$

Following [Shi et al. 2016], we have the following options in a LoG implementation: We may batch modes yielding a non-free index i , denoted with $[i]$, we may flatten modes yielding a single free index, denoted with (ij) , and we may transpose modes, denoted with A_{ij}^T . Note that transposes may only be applied to exactly 2 free modes.

A possible LoG implementation would be

$$C_{(ab)[c](ij)[k]} = \sum_m B_{m[k](ab)}^T A_{(ij)m[c]}^T. \quad (1)$$

That is, we loop over the indices c and k . Inside the loop, GEMM is called for subtensors of C , B , and A . An implementation of Equation (1) is listed in [Springer and Bientinesi 2018, Listing 8].

3 TENSORS IN DISCONTINUOUS GALERKIN METHODS

The discontinuous Galerkin method has become a popular method for solving hyperbolic PDEs. The DG method has several advantages compared to other classic methods, such as Finite Difference methods, Finite Volume methods, and continuous Finite Element methods: It simultaneously allows to handle complex geometries, achieves high-order convergence rates, and has an explicit semi-discrete form [Hesthaven and Warburton 2008]. Additionally, the high number of element-local operations and the small stencil make it a promising candidate to exploit the capabilities of modern supercomputing hardware. Before discussing the details of our tensor toolbox, we want to motivate why tensor contractions are a natural abstraction for DG methods.

As an example, we consider the following linear system of PDEs:

$$\frac{\partial q_p}{\partial t} + A_{pq} \frac{\partial q_q}{\partial x} + B_{pq} \frac{\partial q_q}{\partial y} + C_{pq} \frac{\partial q_q}{\partial z} = 0. \quad (2)$$

Multiplying the latter equation with a test function ϕ_k , integrating over a domain Ω , and integrating by parts yields the corresponding weak form

$$\int_{\Omega} \phi_k \frac{\partial q_p}{\partial t} dV + \int_{\partial\Omega} \phi_k (n_x A_{pq} + n_y B_{pq} + n_z C_{pq}) q_q dS + \int_{\Omega} \left(\frac{\partial \phi_k}{\partial x} A_{pq} q_q + \frac{\partial \phi_k}{\partial y} B_{pq} q_q + \frac{\partial \phi_k}{\partial z} C_{pq} q_q \right) dV = 0, \quad (3)$$

where (n_x, n_y, n_z) is the outward-pointing normal vector. From here a sequence of steps follows to obtain a semi-discrete form, such as partitioning the domain Ω in finite elements Ω_i (e.g. tetrahedra or hexahedra), introducing a numerical flux to weakly couple the finite elements, transforming the physical elements to a reference element, and introducing a polynomial approximation of the quantities on the reference element [Atkins and Shu 1998; Dumbser and Käser 2006; Hesthaven and Warburton 2008]. After these steps, the semi-discrete form is a system of ODEs, which may, for example, be solved with a Runge-Kutta scheme or the ADER approach [Dumbser and Käser 2006].

We skip some steps for simplicity, and assume that the quantities are discretised as $q_p = Q_{lp} \phi_l(x, y, z)$ at a given point in time on an element Ω_i . Here, $\phi_l(x, y, z)$ are a set of \mathcal{B} polynomial basis functions and Q is a $\mathcal{B} \times P$ matrix, storing the coefficients of the basis expansion for every quantity, where P is the number of quantities. By inserting our discretisation we may write the second line of (3) in the following way

$$Q_{lq} A_{pq} \int_{\Omega_i} \frac{\partial \phi_k}{\partial x} \phi_l dV + Q_{lq} B_{pq} \int_{\Omega_i} \frac{\partial \phi_k}{\partial y} \phi_l dV + Q_{lq} C_{pq} \int_{\Omega_i} \frac{\partial \phi_k}{\partial z} \phi_l dV. \quad (4)$$

The integrals in (4) may be pre-computed and stored as (so-called) stiffness matrices K^x , K^y , and K^z of size $\mathcal{B} \times \mathcal{B}$.¹ The implementation in terms of GEMM is then given by the sequence of matrix chain products $K^x Q A^T + K^y Q B^T + K^z Q C^T$.

When one uses the unit cube as reference element, then it is possible to use a spectral basis, where the basis functions and test function are given by $\phi_{k(x,y,z)} = \psi_x(x) \psi_y(y) \psi_z(z)$. The degrees of freedom are then stored in a 4-dimensional tensor Q , such that $q_p = Q_{lmnp} \psi_l(x) \psi_m(y) \psi_n(z)$. In each dimension we have $N + 1$ basis functions, where N is the polynomial degree, and Q has $(N + 1)^3 P$ entries. Inserting the discretisation and the test functions in the second line of (3), we obtain

$$Q_{lmnq} A_{pq} K_{xl} M_{ym} M_{zn} + Q_{lmnq} A_{pq} M_{xl} K_{ym} M_{zn} + Q_{lmnq} A_{pq} M_{xl} M_{ym} K_{zn},$$

¹Note that these matrices need to be only computed for the reference element in an actual implementation.

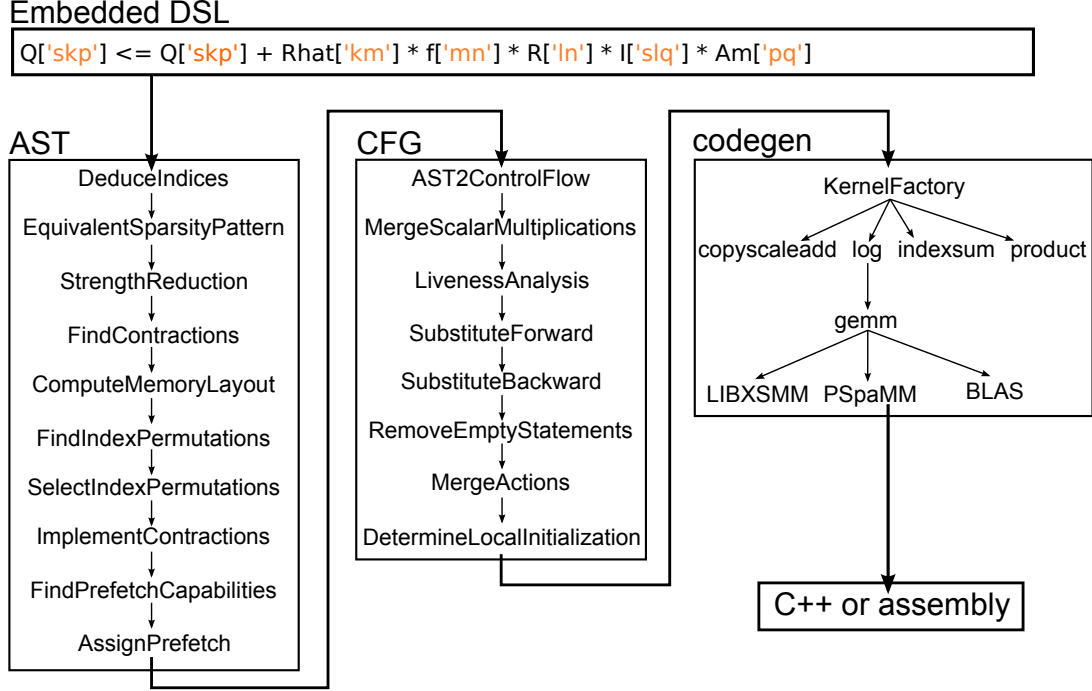


Fig. 1. Overview of YATeTo, showing the path from the high-level language to the generated code. The first stage (left box) operates on an abstract syntax tree, in the second stage (middle box) the representation is changed to a simple control flow graph without branches, and in the last stage (right box) different back-ends are called which output C++ or assembly.

where $K_{ij} = \int_0^1 \frac{\partial \psi_i}{\partial x} \psi_j dx$ and $M_{ij} = \int_0^1 \psi_i \psi_j dx$. We note here that the index order lmn is chosen arbitrarily. In fact, the index permutations $plmn$, $lpmn$, and $lmpn$ are equally viable, and it depends on the application which is best. E.g. if P is large and $N + 1$ is smaller than the SIMD vector width then it might be beneficial to store index p continuous in memory. Otherwise, if $N + 1$ is large and P is small then either of lmn should be continuous in memory.

As a final example, one may solve multiple problems concurrently. E.g. one may add another dimension to the degrees of freedom Q_{lp} in (4) to obtain a 3D tensor Q_{slp} , which stores multiple degrees of freedom [Breuer et al. 2017]. The matrix chain product $K^x Q A^T$ then becomes the tensor contraction sequence $K_{kl}^x Q_{slq} A_{pq}$ and may be implemented using the Loop-over-GEMM approach, e.g. $(Q_{(sl)q} A_{pq}^T)_{sl[p]} (K_{kl}^x)^T$.

4 YET ANOTHER TENSOR TOOLBOX

The input to our tensor toolbox is a domain-specific language (DSL), which naturally resembles the Einstein notation. An abstract syntax tree (AST) is derived from an expression. Subsequently, the tree is shaped using a sequence of visitors [Gamma et al. 1995]. Afterwards, we transform the AST to a control flow graph (CFG) for standard compiler techniques [Seidl et al. 2012]. Note that the CFG is very simple as the DSL does not feature loops and branches. Finally, a code generator is called which generates either C++-11 code or may make use of existing code generators or BLAS libraries. An overview is shown in Figure 1. YATeTo is open-source and available on www.github.com/SeisSol/yateto.

In the following, we are going to introduce our DSL and elaborate algorithms and design choices of each of the three stages.

4.1 High-level description of tensor operation

The DSL we created is embedded into Python 3. An embedded DSL has the advantage that we do not need our own parser and lexer, which decreases the complexity of the software. Furthermore, a user may use any feature of Python to form expressions, for example including loops, branches, classes, and lambda expressions.

The basic data types are the classes Tensor and Scalar. A tensor definition includes a name and a shape tuple, e.g. as in the following:

```
N = 8
A = Tensor('A', (N, N))
B = Tensor('B', (N, N, N))
w = Tensor('w', (N,))
C = Tensor('C', (N, N))
```

A and C are matrices, B a third order tensor, and w is a vector, where all dimensions are of size N.

From a Tensor, an object of type IndexedTensor may be derived by supplying an index string. The convention is that the length of the index string must be equal to the number of dimensions of the tensor and that only lower- and upper-case letters may be used.² Objects of type IndexedTensor may appear in expressions, e.g.

```
kernel = C['ij'] <= 2.0 * C['ij'] + A['lj'] * B['ikl'] * w['k']
```

The design is inspired by [Solomonik et al. 2013] (see Section 2.1), and represents the operation

$$C_{ij} := 2 \cdot C_{ij} + \sum_{l=0}^{N-1} \sum_{k=0}^{N-1} A_{lj} B_{ikl} w_k \quad \text{or equivalently} \quad C := 2 \cdot C + (B \times_2 w)A.$$

The variable kernel contains an AST with nodes Assign, Add, ScalarMultiplication, and Einsum, where the latter represents a tensor operation using the Einstein convention.

The AST is built by overloading the binary operators '*' and '+'. One of the following four actions is taken whenever one of the operators is invoked for operands op1 and op2, where nodeType = Einsum for '*' and nodeType = Add for '+':

- (1) type(op1) = nodeType and type(op2) = nodeType: Append op2's children to op1.
- (2) type(op1) = nodeType and type(op2) ≠ nodeType: Append op2 to op1.
- (3) type(op1) ≠ nodeType and type(op2) = nodeType: Prepend op1 in op2.
- (4) type(op1) ≠ nodeType and type(op2) ≠ nodeType: Return nodeType of op1 and op2.

These actions ensure that a node of type nodeType does not have children of type nodeType, but all tensors w.r.t. the same nodeType are merged. This is important, especially for Einsum and the algorithms presented in Section 4.2 and Section 4.3, which require all tensors participating in a tensor operation to be known. Note that we do not apply distributive laws, e.g. in the expression $\sum_k A_{ik}(B_{kj} + C_{kj})$ the addition is always evaluated before the Einstein sum.

For scalar multiplications we take similar actions to ensure that ScalarMultiplication is always the parent node of an Einsum.

4.2 Equivalent sparsity patterns

The notion of equivalent sparsity patterns (EQSPPs) and an algorithm to compute them was introduced in [Uphoff and Bader 2016] for matrix chain products (MCP). It is defined as the minimal sparsity patterns of the involved matrices that

²Note that this limits the number of distinct indices that may appear in an expression to 52. We think that this is not an issue in practice, hence we favour simplicity instead of generality.

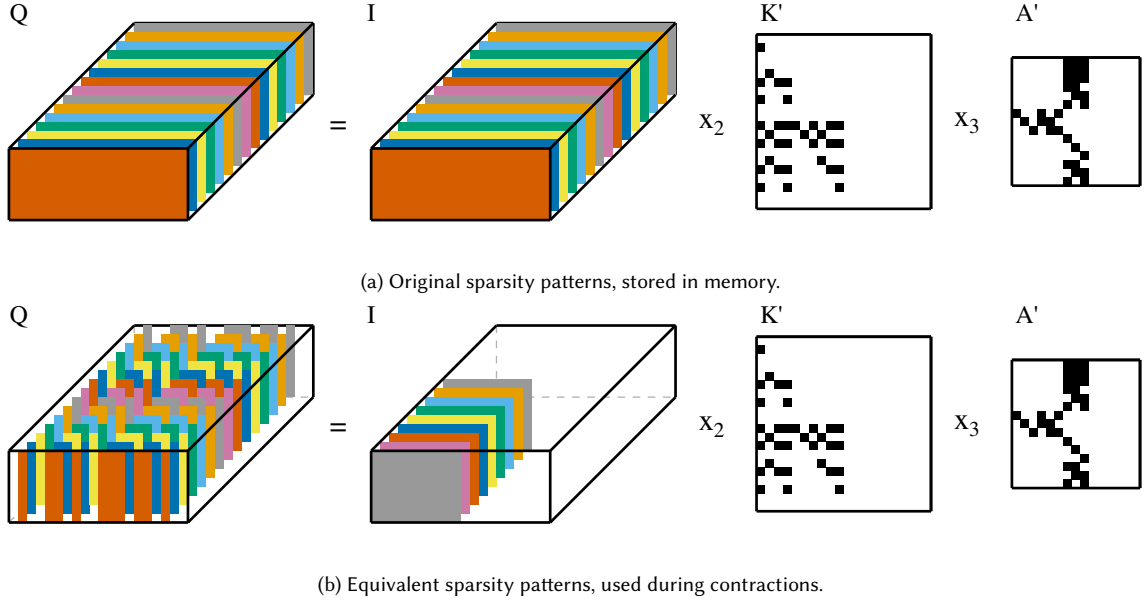


Fig. 2. We show the kernel $Q_{skp} = I_{slq} K_{lk} A_{qp}$ (depicted with mode-n product, i.e. $Q = I \times_2 K^T \times_3 A^T$), which is similar to an application example in [Uphoff and Bader 2016] but with an additional dimension added to the degrees of freedom. The degrees of freedom (I , Q) are given as full tensor (Figure 2a), but we detect that large blocks in I do not influence the final result, as they are multiplied with zeros in the tensor contractions (Figure 2b).

leaves the result of an MCP unchanged. In the latter definition, no cancellation is assumed, which means that adding non-zero entries never results in zero [Cohen 1998]. First, the assumption allows to work with boolean matrices alone. Second, we assume that the sparsity pattern is known but the values are unknown (or known only at run-time), which has the following implication: In an inner product, which is the core of matrix multiplication, we can always find a pair of non-orthogonal vectors. That is, if the values of at least one matrix are unknown, we cannot guarantee cancellation.

The concept of EQSPPs can be illustrated with the following example (where the entries may be either scalars or dense block matrices):

$$\begin{pmatrix} K_1 & 0 \\ 0 & 0 \end{pmatrix} \begin{pmatrix} Q_{11} & Q_{12} \\ Q_{21} & Q_{22} \end{pmatrix} \begin{pmatrix} A_1 \\ 0 \end{pmatrix} = K_1 Q_{11} A_1$$

Here, the multiplication with the first matrix removes Q_{21} and Q_{22} from the right-hand side and the multiplication with the third matrix removes Q_{12} and Q_{22} from the right-hand side. Thus, the equivalent sparsity pattern of the second matrix is only non-zero for the top-left block (Q_{11}).

In [Uphoff and Bader 2016] an algorithm to compute EQSPPs for MCPs is presented, which is based on a graph based representation. The extension of the MCP graph to general tensor operations is not straightforward, thus we derive an algorithm that is not based on a graph in the remainder of this section.

4.2.1 Formalisation of tensor operations. So far we have defined tensor operations via handwaving and examples, but here we need to introduce a formal definition of the “ \ast ”-expression in our DSL.

First of all, we formalise the labelling of the dimensions of a tensor T . It consists of a set of indices and an assignment of indices to dimensions. We denote the set of indices with calligraphic letters, e.g. $\mathcal{T} \subset \mathcal{P}(\Sigma)$, which must be a

subset of the power-set of an alphabet Σ , where e.g. $\Sigma = \{a, \dots, z\}$. We require $|\mathcal{T}| = \dim(T)$.³ The assignment of indices to dimensions is a bijective mapping $P_T : \mathcal{T} \rightarrow \{1, \dots, \dim(T)\}$. The range of an index i is always $I_{P_T(i)} := \{0, \dots, \text{size}(i) - 1\}$, where $\text{size}(i) \in \mathbb{N}$.

EXAMPLE 1. Let $A \in \mathbb{R}^{2 \times 2 \times 2}$. The index set of $A[\text{'ijk'}]$ is $\mathcal{A} = \{i, j, k\}$, the map P_A is given by $P_A(j) = 1, P_A(i) = 2, P_A(k) = 3$, and $\text{size}(i) = \text{size}(j) = \text{size}(k) = 2$.

Second, assume a “*”-expression is formed by n tensors T^1, \dots, T^n , and the result tensor U . Einstein’s convention requires us to sum over all indices that appear twice, which we formalise in the following: The index space of tensor T^k is $\mathbb{S}(T^k) = I_1 \times \dots \times I_{\dim(T^k)}$, where $I_d \subset \mathbb{N}_0$ is the index range of the d -th dimension. In order to span an iteration space, we introduce the global index set $\mathcal{G} = \bigcup_k \mathcal{T}^k$, and the global index space $\mathbb{G} = \times_{k=1}^N \{0, \dots, \text{size}(P_G^{-1}(k)) - 1\}$, where $N = |\mathcal{G}|$. Similar to a tensor, we assign global indices to dimensions of the global index space with the bijective function $P_G : \mathcal{G} \rightarrow \{1, \dots, N\}$.⁴ In order to “access” entries of a tensor, we introduce projection and permutation functions $\pi_{T^k} : \mathbb{G} \rightarrow \mathbb{S}(T^k)$, where

$$\pi_{T^k}(i_1, \dots, i_N) = \left(i_{P_G^{-1}(d)} : 1 \leq d \leq |\mathcal{T}^k| \right).$$

Entries of T^k are accessed with the notation $T^k[\pi_{T^k}(i)]$, where $i \in \mathbb{G}$, or shortly with T_{π}^k , where the permutation and projection function is understood from context. We define the restriction of the global index set to an index $i \in \mathbb{S}(T)$ as $R_T(i) = \{j \in \mathbb{G} : \pi_T(j) = i\}$.

With the set up formalism, we are able to precisely state the meaning of a “*”-expression:

$$\forall i \in \mathbb{S}(U) : U_i = \sum_{j \in R_U(i)} T_{\pi_j}^1 \cdot \dots \cdot T_{\pi_j}^n. \quad (5)$$

EXAMPLE 2. Consider tensors $A \in \mathbb{R}^{2 \times 2 \times 2}$ and $B \in \mathbb{R}^{2 \times 2}$. In Einstein notation, the mode-2 product is written as $C_{ijk} = A_{i1k} B_{j1}$ and in our DSL as $C[\text{'ijk'}] \leftarrow A[\text{'i1k'}] * B[\text{'j1'}]$.

In our formal notation, the global index space is $\mathbb{G} = I \times J \times K \times L$, where $I = J = K = L = \{0, 1\}$. The permutation and projection functions are $\pi_A : (i, j, k, l) \mapsto (i, l, k)$, $\pi_B : (i, j, k, l) \mapsto (j, l)$, and $\pi_C : (i, j, k, l) \mapsto (i, j, k)$. We may compute the entries of C with

$$(i, j, k) \in I \times J \times K : C_{(i,j,k)} = \sum_{(i',j',k',l') \in \{i\} \times \{j\} \times \{k\} \times L} A_{(i',l',k')} B_{(j',l')}.$$

4.2.2 Computation of EQSPPs for tensor operations. As we assume no cancellation in sums, it is sufficient to model a sparsity pattern as a boolean tensor. The EQSPP of a tensor T^k is called $\hat{\Theta}^k$, where $\hat{\Theta}_q^k \in \{0, 1\}$, $q \in \mathbb{S}(T^k)$. The “hat”-tensor \hat{T}^k is the original tensor T^k masked with $\hat{\Theta}^k$. In operations involving $\hat{\Theta}^k$ we identify $+$ with \vee and \cdot with \wedge .

Having set up the necessary formalism, we are ready to formally define EQSPPs:

Definition 4.1. Assuming no cancellation, we call $\hat{\Theta}^k$ equivalent sparsity patterns w.r.t. (5) if

$$(1) U = \hat{U}, \text{ where } \forall i \in \mathbb{S}(U) : \hat{U}_i = \sum_{j \in R_U(i)} \hat{T}_{\pi_j}^1 \cdot \dots \cdot \hat{T}_{\pi_j}^n \text{ and } \hat{T}_q^k = \begin{cases} T_q^k & \text{if } \hat{\Theta}_q^k = 1 \\ 0 & \text{if } \hat{\Theta}_q^k = 0. \end{cases}$$

³Note that this requirement excludes the trace of a matrix T_{ii} or similar expressions. However, one may write the trace as $T_{ij} \delta_{ij}$, which conforms with the requirement.

⁴The function P_G may for example be obtained by ordering the global index set lexically.

- (2) The number of non-zeros of $\hat{\Theta}^k$, $k = 1, \dots, n$, is minimal, that is, we cannot set a non-zero to zero without implying $\exists i \in \mathbb{S}(U) : U_i \neq \hat{U}_i$.

As we assume no cancellation, we may disregard the sums over indices, and instead need to only consider a product over all tensors on the right-hand side:

LEMMA 1. *The EQSPPs w.r.t. (5) are equivalent to the EQSPPs w.r.t.*

$$\forall j \in \mathbb{G} : Z_j := T_{\pi_j}^1 \cdot \dots \cdot T_{\pi_j}^n.$$

PROOF. Clearly, $\forall i \in \mathbb{S}(U) : U_i = \sum_{j \in R_U(i)} Z_j = \sum_{j \in R_U(i)} \hat{Z}_j$, hence condition 1 is fulfilled.

In order to check condition 2, assume there is another set of EQSPPs, $\bar{\Theta}^k$, which has less non-zeros than $\hat{\Theta}^k$. Then $\exists f \in \mathbb{G} : Z_f = \hat{Z}_f \neq \bar{Z}_f$ (otherwise \hat{T}^k would not be minimal). As $\bigcup_{i \in \mathbb{S}(U)} R_U(i) = \mathbb{G}$ and Z_f does not get cancelled in sums, it follows that there exists an index $g \in \mathbb{S}(U)$ where $\bar{U}_g \neq U_g$. \square

Our main result is that we may cast the computation of EQSPPs as boolean tensor operations on the original sparsity patterns:

PROPOSITION 1. *The EQSPPs w.r.t. (5) are given by*

$$\forall q \in \mathbb{S}(T^k) : \hat{\Theta}_q^k := \sum_{l \in R_{T^k}(q)} \Theta_{\pi_l}^1 \cdot \dots \cdot \Theta_{\pi_l}^n, \quad (6)$$

where Θ^l is the sparsity pattern of T^l , $l = 1, \dots, n$.

PROOF. We are going to show that (6) computes the EQSPPs for the product Z of tensors T^1, \dots, T^n (see Lemma 1). In order to satisfy condition 1, we only need to show that the sparsity patterns of Z and \hat{Z} are identical. The sparsity pattern of Z is given by ζ , where $\forall j \in \mathbb{G} : \zeta_j := \Theta_{\pi_j}^1 \cdot \dots \cdot \Theta_{\pi_j}^n$, and the sparsity pattern of \hat{Z} is given by $\hat{\zeta}$, where $\forall j \in \mathbb{G} : \hat{\zeta}_j := \hat{\Theta}_{\pi_j}^1 \cdot \dots \cdot \hat{\Theta}_{\pi_j}^n$.

First, we show that $\forall j \in \mathbb{G} : \hat{\zeta}_j = \zeta_j$. Note that

$$\hat{\Theta}_q^k = \sum_{l \in R_{T^k}(q)} \Theta_{\pi_l}^1 \cdot \dots \cdot \Theta_{\pi_l}^n = \sum_{l \in R_{T^k}(q)} \zeta_l = \Theta_q^k \cdot \sum_{l \in R_{T^k}(q)} \zeta_l, \quad (7)$$

where the latter equality follows from idempotence and $\Theta_{\pi_l}^k = \Theta_q^k$ if $l \in R_{T^k}(q)$ by the definition of R_{T^k} . Using (7) we obtain

$$\hat{\zeta}_j = \hat{\Theta}_{\pi_j}^1 \cdot \dots \cdot \hat{\Theta}_{\pi_j}^n = \zeta_j \cdot \left(\sum_{l \in R_{T^1}(\pi_{T^1}(j))} \zeta_l \right) \cdot \dots \cdot \left(\sum_{l \in R_{T^n}(\pi_{T^n}(j))} \zeta_l \right) = \zeta_j, \quad (8)$$

where the last identity follows from $j \in R_{T^k}(\pi_{T^k}(j))$ and the absorption law. Equation (8) is true for all $j \in \mathbb{G}$, hence $\zeta = \hat{\zeta}$.

Second, in order to satisfy condition 2, we show that the number of non-zeros is minimal: Assume that there exist another set of sparsity patterns $\bar{\Theta}^k$, with less non-zeros than $\hat{\Theta}^k$. Then, $\exists k \in \{1, \dots, n\} : \exists q \in \mathbb{S}(T^k) : \bar{\Theta}_q^k = 0 \wedge \hat{\Theta}_q^k = 1$. Clearly, $\Theta_q^k = 1$ and $\sum_{l \in R_{T^k}(q)} \zeta_l = 1$, because otherwise $\hat{\Theta}_q^k \neq 1$. Hence, there must be at least one $p \in R_{T^k}(q)$ such that $\zeta_p = 1$. As $\pi_{T^k}(p) = q$ it immediately follows that

$$\bar{\zeta}_p := \bar{\Theta}_{\pi_p}^1 \cdot \dots \cdot \bar{\Theta}_{\pi_p}^{k-1} \cdot \bar{\Theta}_q^k \cdot \bar{\Theta}_{\pi_p}^{k+1} \cdot \dots \cdot \bar{\Theta}_{\pi_p}^n = 0 \neq \zeta_p = 1,$$

which violates condition 1. \square

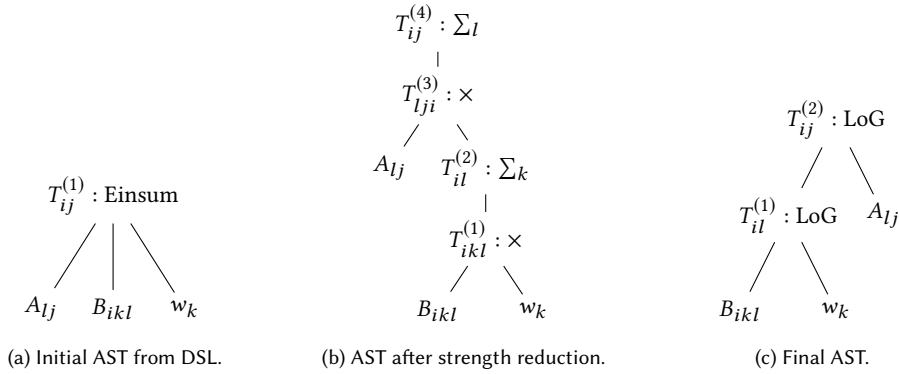


Fig. 3. Overview of major stages during AST transformation of an Einsum node (left). After determining the equivalent sparsity patterns, the Einsum node is transformed during strength reduction, yielding an operation-minimal tree (middle). This tree is binary and consists of Product and IndexSum nodes only. Finally, a mapping to Loop-over-GEMM is found which minimises the cost function described in Section 4.5 (right).

4.2.3 Implementation and discussion. We have applied our EQSPP algorithm to an application example from [Uphoff and Bader 2016], where we extended the degrees of freedom by an additional dimension (cf. Section 5.1). The original SPPs and EQSPPs can be seen in Figure 2. We observe that the non-zero entries of K and A induce additional zeros in I which may be disregarded when computing the tensor operation. For example, in the evaluation of $I_{slq}K_{lk}$ we may restrict the loop ranges of q and l .

The implementation of EQSPP-computation with (6) is straightforward, as we require the same kind of tensor operations that we support within YATeTo, the only difference being that the tensors are boolean. E.g. we may apply strength reduction (cf. Section 4.3) in order to reduce the amount of computations. Still, our method to compute EQSPPs is more expensive to compute than to simply evaluate the original tensor operation. Nevertheless, the cost of computing EQSPPs is negligible in comparison to the possibly millions of times a kernel is called within a DG scheme.

4.3 Strength reduction

We already mentioned in Section 4.3 that finding the sequence of tensor operations with minimal operation count is an NP-hard problem, but an efficient enumeration procedure exists for tensor dimensions appearing in practice [Lam et al. 1997]. The same enumeration procedure may also be used when sparse tensors are involved, but in this case the sparsity patterns of intermediate results are required, or at least an estimate of the sparsity [Lam et al. 1999].

In YATeTo we assume that tensors are small enough, such that it is feasible to explicitly compute all intermediate products during strength reduction. The number of operations is then determined in the following way [Lam et al. 1999]: For a multiplication formula $V[\dots] = X[\dots] \times Y[\dots]$ the number of operations is equal to the number of non-zeros in V . For a summation formula $W[\dots] = \sum_i Z[\dots]$ the number of operations is equal to the number of non-zeros in Z minus the number of non-zeros in W .

An example of an intermediate AST after strength reduction is shown in Figure 3b.

4.4 Memory layouts

Following Figure 1 the next step is to compute memory layouts of tensors. The memory layout influences the possibility to fuse indices in a LoG-implementation. Thus the layout influences the cost function in Section 4.5 and needs to be fixed at this point already. In the following we give an overview over the two classes of memory layouts that are currently supported.

4.4.1 Dense layout. Let $A \in \mathbb{R}^{n_1 \times n_2 \times \dots \times n_d}$. We call the tuple (n_1, n_2, \dots, n_d) the shape of a tensor. A simple memory layout of a dense tensor is the “column-major” storage:

$$A_{i_1 \dots i_d} := A \left[\sum_{k=1}^d i_k s_k \right],$$

where the so-called stride is given by $s_k = \prod_{l=0}^{k-1} n_l$ with $n_0 := 1$. That is, the tensor is stored linearly in a 1D array, such that the first dimension varies fastest and the last dimension varies slowest in memory. The stride s_k gives us the number of floating numbers we have to skip when we increase index i_k by one.

From Section 4.2 we expect that we also have tensors with large zero blocks, where it would be wasteful to store the full tensor. Hence, our next evolution is the bounding-box column-major storage:

$$A_{i_1 \dots i_d} := A \left[\sum_{k=1}^d (i_k - b_k) t_k \right],$$

where $t_k = \prod_{l=0}^{k-1} (B_l - b_l)$ and $0 \leq b_k < B_k \leq n_k$. This memory layout models the case where A is non-zero within the index set $[b_1, B_1) \times \dots \times [b_d, B_d)$ and zero otherwise.

Finally, it might be beneficial to align the fastest dimension. That is, the number of bytes in a fibre in the first dimension should be divisible by the architecture’s SIMD vector length. In some cases, one has to add artificial zeros to the first dimension, hence we allow that the bounding interval of the first dimension is larger than the size of the first dimension. Given an initial (minimal) bounding interval $[b_1, B_1)$ we align the bounding interval as in [Uphoff and Bader 2016], that is,

$$[b'_1, B'_1) := [b_1 - b_1 \bmod v, B_1 + (v - B_1 \bmod v) \bmod v),$$

where v is the number of floating point values that fit into a SIMD vector (e.g. using AVX-512 one sets $v = 8$ for double precision or $v = 16$ for single precision).

We conclude the presentation of dense layouts with a possible pitfall of using bounding boxes and alignment. It might be beneficial to fuse multiple indices when mapping a tensor contraction to a Loop-over-GEMM (see Section 2.3). Fusing indices $i_a \dots i_b$ is always possible when [Shi et al. 2016]

$$\forall i \in [a, b) : t_{i+1} = n_i t_i. \tag{9}$$

Other cases would require more involved compatibility conditions. For example in the GEMM $C_{(ij)(kl)} = A_{(ij)m} B_{m(kl)}$, where artificial zeros are added for dimension i in A and dimension k in B , then one may only fuse (ij) and (kl) whenever C has the same number of artificial zeros in dimension i and k . Otherwise one needs temporary storage and an additional data copy. In order to avoid possible data copies and complications arising in subsequent optimisation steps we only allow fused indices when (9) is fulfilled. Conversely, aligned layouts or bounding box layouts have to be considered carefully as they may prohibit fusing indices, which leads to smaller (and possibly slower) GEMMs.

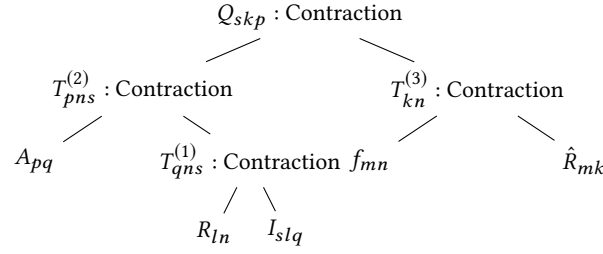


Fig. 4. A possible intermediate AST of $Q_{skp} := \hat{R}_{km}f_{mn}R_{ln}I_{slq}A_{pq}$. We have the freedom to choose the index permutations of the temporary tensors $T^{(1)}$, $T^{(2)}$, and $T^{(3)}$.

4.4.2 Compressed sparse column (CSC) layout. Sparse matrices may appear in discontinuous Galerkin methods, e.g. the stiffness matrices are sparse when an orthogonal set of basis functions is used. We have a limited support for the CSC format: CSC matrices may appear in GEMM or Loop-over-GEMM calls but only in a sparse x dense or a dense x sparse GEMM.

4.4.3 Other (sparse) formats. It might be surprising that we describe Equivalent Sparsity Patterns in great detail but currently do not offer a genuine sparse tensor memory layout. First of all, we want to point out that if an EQSPP induces a large zero block, then we are able to exploit this block using the bounding box memory layout or we may let a LoG operate only on a subtensor. Second, to the authors' knowledge, an efficient code generator or efficient routines for general small sparse tensors do currently not exist.

4.5 Optimal index permutations

The strength reduction step converts each Einsum node to a binary tree consisting only of IndexSum and Product nodes. In a first step, we identify contractions in the tree, which are (multiple) IndexSum nodes followed by a single Product node. A sub-tree that was identified to be a contraction is replaced by a new node of type Contraction. For example, we might end up with the (sub-)tree shown in Figure 4.

Each Contraction node shall now be mapped to an implementation as Loop-over-GEMM. In general, the mapping to GEMM is not unique, but several implementations are possible (e.g. [Shi et al. 2016, Table II]). A systematic way to list all possible implementations is given in [Springer and Bientinesi 2018, Listing 7]. As accurately predicting the performance of each implementation is difficult, heuristics may be employed to select the most promising candidate, e.g. one may choose the variant with the largest GEMM [Springer and Bientinesi 2018].

The algorithm to list all LoG-implementations in [Springer and Bientinesi 2018] assumes that the order of all indices are known. In our case we have temporary tensors in which an order of indices is not prescribed. (E.g. $T^{(1)}$, $T^{(2)}$, and $T^{(3)}$ in Figure 4.) The index order has to be chosen carefully as it decides possible mappings to GEMM and there are even cases where non-unit stride GEMMs are required [Shi et al. 2016, Table II]. Moreover, the index order of a temporary result influences possible mappings to GEMM in nodes that involve the temporary result.

4.5.1 Optimal index permutations. Our approach to select the index orders of temporary tensors is to solve the following discrete optimisation problem: Let $\mathcal{V}(r)$ be the set of vertices of an AST with root r . We denote the set of children of a vertex v with $C(v)$, and the set of descendants of a vertex v with $\mathcal{D}(v) = \mathcal{V}(v) \setminus \{v\}$. For each vertex v we have a set of permissible index permutations \mathcal{P}_v . We introduce variables x_v , for all $v \in \mathcal{V}(r)$, where $x_v \in \mathcal{P}_v$ i.e. variable

x_v contains the index permutation for vertex v . The Cartesian product of all permissible index permutations is called the configuration space. The optimisation problem is to find a configuration which minimises a cost function over all possible configurations, that is,

$$c^* = \min_{x_r \in \mathcal{P}_r, x \in S} W(x_r, x), \quad \text{where } S = \prod_{v \in \mathcal{D}(r)} \mathcal{P}_v. \quad (10)$$

We define the cost function of a tree with root r recursively in the following way:

$$W(x_r, x) = w_r(x_r, (x_c)_{c \in C(r)}) + \sum_{c \in C(r)} W(x_c, (x_d)_{d \in \mathcal{D}(c)}). \quad (11)$$

The functions w_r can be thought of as a measure of the cost of the operation represented by a vertex in the AST. We give a detailed definition of w_r in Section 4.5.2.

We split the minimisation in two stages. In the first stage we minimise over the root variable and its children, in the second stage we minimise over all other variables, i.e. the variables associated with the vertices in the set $\mathcal{G}(r) = \bigcup_{c \in C(r)} \mathcal{D}(c)$. One can then show that

$$\begin{aligned} c^* &= \min_{x_r, (x_c)_{c \in C(r)}} \min_{(x_d)_{d \in \mathcal{G}(r)}} W(x_r, (x_d)_{d \in \mathcal{D}(r)}) \\ &= \min_{x_r, (x_c)_{c \in C(r)}} \left(w_r(x_r, (x_c)_{c \in C(r)}) + \sum_{c \in C(r)} f_c(x_c) \right), \end{aligned}$$

where we introduced

$$f_c(y) = \min_{(x_d)_{d \in \mathcal{D}(c)}} W(y, (x_d)_{d \in \mathcal{D}(c)}). \quad (12)$$

The sub-problem introduced in (12) can be interpreted as finding the optimal configuration for a sub-tree, assuming that the index permutation of the root node is fixed. In fact, $c^* = \min_{x_r \in \mathcal{P}_r} f_r(x_r)$. Such problems are said to have an optimal substructure, because the optimal solution can be constructed out of optimal solutions to sub-problems [Cormen et al. 2009].

Dynamic programming is a commonly used approach for problems with optimal substructure. We consider a bottom-up dynamic programming algorithm, which works in the following way: The AST is traversed in post-order. For each vertex v , we solve problem (12) for every permissible index permutation $x_v \in \mathcal{P}_v$. The minimum cost as well as a minimising configuration is memoized in a dictionary. If vertex v is a leaf node, we simply evaluate all index permutations in \mathcal{P}_v . For internal nodes, we evaluate all configurations in $\mathcal{P}_v \times (\prod_{w \in C(v)} \mathcal{P}_w)$. In order to evaluate the cost, we evaluate the function w_v and for the sub-problems we look-up the memoized costs. (The latter are available due to the post-order traversal.) The run-time of this algorithm can be bound with $O(N(n!)^{1+c})$, where N is the number of vertices in an AST, n is the maximum number of indices in a vertex (and hence $n!$ is the maximum size of each permissible index permutation set), and c is the maximum number of children.

4.5.2 Cost function. The missing pieces in the last section are the cost functions w_r . Here, we choose a simple heuristic. Our basic assumption is that our ASTs will consist mostly of LoGs and that those will dominate the run-time. Hence, all other operations are assigned cost zero. Further assumptions are listed in the following:

- Non-unit stride GEMMs are inferior to unit stride GEMMs.

- Transposes of $A(B)$ in the GEMM AB should be avoided when using column-major (row-major) layout. Transposes of $B(A)$ should be avoided due to missing support in code generation back-ends.
- Large GEMMs are faster than small GEMMs, i.e. one should fuse as many indices as possible.

From these assumptions we define the cost of a LoG as the 4-tuple $(s, l, r, -f)$, where s is the number of required slices with non-unit stride, l is the number of left-transposes (assuming column-major layout), r is the number of right-transposes, and f is the number of fused indices. Cost comparison is based on lexicographic comparison of $(s, l + r, -f)$, where the lower number of left-transposes is deciding when two 3-tuples are equal.

The cost function is then

$$w_r(x_r, (x_c)_{c \in C(r)}) = \begin{cases} \text{MinLoG}(x_r, (x_c)_{c \in C(r)}) & \text{if } \text{type}(x_r) = \text{LoG}, \\ (\infty, \infty, \infty, \infty) & \text{if } \text{type}(x_r) \neq \text{LoG} \wedge \text{violated constraints}, \\ (0, 0, 0, 0) & \text{else,} \end{cases}$$

where MinLoG enumerates feasible LoG-implementations and returns a LoG-implementation with minimum cost or infinite cost if no mapping exists. With “violated constraints” we summarise additional constraints that exist, e.g. for Add or Assign nodes.

4.5.3 Discussion. The cost function we employ is clearly limited, as it is a heuristic and makes sense for LoG nodes only. However, choosing another cost function does not change the dynamic programming scheme, as long as the cost function is structurally equivalent to Equation (11). For example, one could swap our LoG-cost by a run-time model based on micro-benchmarks, using the methods developed in [Peise and Bientinesi 2012].

The algorithm needs to visit every node only once, hence the algorithm is feasible also for large ASTs. Problematic are tensors with many dimensions (say large n), as the number of permutations is $n!$ and we need to check all of them. But as stated in the introduction, we assume that our tensors fit into low-level caches, which constrains n . E.g. $n = 6$ is the maximum number of dimensions we may choose such that a 4^n tensor (double precision) still fits into a 32 KiB L1 cache. In other words, YATeTo is not designed for high-dimensional tensors.

An example of an AST after mapping to LoG can be seen in Figure 3c.

4.6 Prefetching

The library LIBXSMM, a generator for small matrix matrix multiplications, allows software prefetching instructions to be included in the generated assembler code [Heinecke et al. 2016b]. This may improve performance, particularly on Intel Knights Landing architecture [Heinecke et al. 2016a; Uphoff et al. 2017]. A possible prefetching strategy is to insert `vprefetch1` instructions for a matrix B after writes to the result matrix C, where the memory offset calculated for the matrix C are also used for the matrix B. The rationale is that B has the same or a similar shape as C.

In YATeTo the users may add a list of tensors they wish to be prefetched to a kernel. The `FindPrefetchCapabilities` visitor determines the number of bytes that may be prefetched for every node of the kernel. For a LoG-node this is equal to the number of bytes in the result tensor. (Other nodes have no prefetch capability, but this may be added if appropriate code generators are available.) `AssignPrefetch` then greedily assigns each to-be-prefetched tensor P to one of the nodes, such that the number of bytes of P matches the prefetch capability of the node.

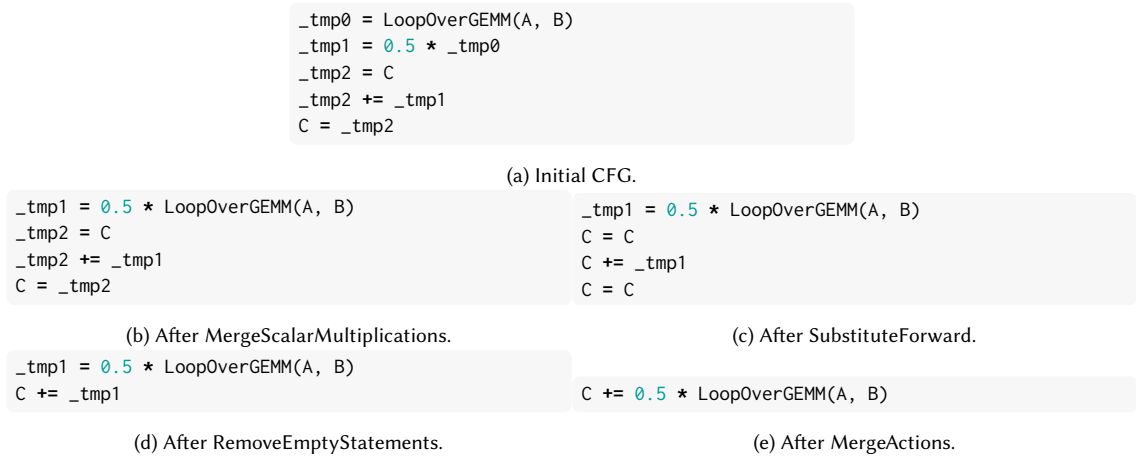


Fig. 5. Illustration of CFG optimisation of a matrix multiplication example.

4.7 Control flow graph

Following Figure 1, we convert the AST to a control flow graph (CFG) representation [Seidl et al. 2012]. The aim here is first to obtain a standardised sequential representation for the later code generation step, and second to manage temporary buffers or to avoid them at all.

The data structure of the CFG are program points (vertices), which save the current state of the kernel, and actions (edges), which transform the kernel's state. An action may be either an assignment or a plus-equals operation. The left-hand side is always a tensor. The right-hand side may be either a tensor or one of the operations modelled in the AST (such as LoG or Product). The right-hand side may be augmented by multiplication with a scalar.

The individual optimisation steps use standard techniques from compiler optimisation [Seidl et al. 2012], thus we only briefly summarise them in the following:

- (1) MergeScalarMultiplications: The actions $A = f(\dots); B = \alpha A$ are replaced by $B = \alpha f(\dots)$.
- (2) LivenessAnalysis: Determine live variables [Seidl et al. 2012].
- (3) SubstituteForward: If possible, replace A by tmp after action $A = \text{tmp}$.
- (4) SubstituteBackward: If possible, replace left-hand side tmp by A if there follows an action $A = \text{tmp}$.
- (5) RemoveEmptyStatements: Remove statements such as $A = A$.
- (6) MergeActions: Try to merge actions, e.g. merge $A = f(\dots)$ and $B += A$ to $B += f(\dots)$, when there is no intermediate action which depends on A .
- (7) DetermineLocalInitialization: Greedy map of temporary buffers to temporary variables. If buffers are used for multiple variables, set the buffer size to the maximum size required by its assigned variables.

In order to illustrate the individual steps, we present matrix multiplication as an example:

```
C['ij'] <= C['ij'] + 0.5 * A['ik'] * B['kj']
```

A simple, but correct, traversal of the corresponding AST yields the sequential CFG shown in Figure 5a. This inefficient CFG is transformed to a single call to GEMM (with $\alpha = 0.5$ and $\beta = 1$), as shown in Figure 5e.

4.8 Code generation

The final step is to generate machine code. In principle, the aim is to re-use existing code generators, such as LIBXSMM [Heinecke et al. 2016b] or PSpaMM [Brei 2018; Wauligmann and Brei 2019], or flavours of BLAS. Besides, YATeTo generates C++-glue-code, and it is able to generate generic fallback code, whenever an efficient implementation is not available. The fallback code consists of nested loops and is architecture independent, but we expect the performance to be rather poor and compiler-dependent.

Operations are divided into four types: `copyscaleadd`, `indexsum`, `product`, and `log`. The first type is a combination of the BLAS routines `COPY` and `AXPY`, and may be implemented in terms of these two functions. The `product` and `indexsum` types correspond to the multiplication formulae and summation formulae presented in Section 2.1. Having a generic implementation for these two types ensures that we cover a large class of tensor operations [Lam et al. 1997]. The `log` type implements Loop-over-GEMMs.

Our concept requires that it should be simple to include additional code generators depending on the type of operation and on the architecture. We use the factory method pattern [Gamma et al. 1995] to distinguish between code generators. For each type, the factory method may return a different code generator depending on the operation’s description (e.g. dense or sparse matrices) and the architecture. For the LoG type, YATeTo offers a generic C++-loop-based implementation, which internally calls another factory method for GEMM. But our structure would also allow to call specialised LoG generators, such as the ones developed in [Breuer et al. 2017] for contractions involving 3D tensors and matrices.

4.9 Application interface

A class is generated for every kernel. The class has an argument-free `execute` function and pointers to the input and output tensors of the kernel are public members, where the name of a member variable is given by the name of the tensor. So in order to invoke a kernel one has to create a kernel object, set the pointers to the input and output tensors, and call the `execute` function. A kernel class also stores the following information as static members: The minimal number of flops,⁵ also sometimes called non-zero flops, and the number of flops the implementation requires, also sometimes called hardware flops. The number of non-zero flops is computed by means of strength reduction with the sparse cost function in Section 4.3, and the hardware flops are returned by the code generators. These flop counters are useful to evaluate the performance of the kernels.

In addition to the kernel classes, a unit test is generated for every kernel. The unit test compares the optimised kernel to the naive implementation of the same kernel. If the Frobenius norm of the difference of both implementations matches up to a tolerance, the unit test passes. (We allow a tolerance due to finite arithmetic imprecision caused by the difference in order of addition.)

Moreover, a class is generated for every tensor, where information about the memory layout is stored. The most useful static member, which is declared `constexpr`, is the number of required floating point numbers. This information may be used to allocate stack or heap memory for a tensor. For convenience, each tensor class contains a function that returns a view object for a memory region. Using a view object V the user may access a d -dimensional tensor with operator `()`, i.e. $V(i_1, \dots, i_d)$. Tensors whose entries are known at compile time (e.g. stiffness matrices) may be stored within the generated code as static array, already formatted according to the selected memory layout.

⁵Strictly speaking, the term “minimal” is incorrect due to Strassen’s algorithm or other bounds on the number of operations. That is, minimal is understood as minimal w.r.t. the cost function defined in Section 4.3.

To integrate YATeTo into the build process of an application, users need to have Python 3 and NumPy installed. The generated code follows C++11 syntax and depends on a small header-only library, i.e. the generated code itself requires only a recent C++-compiler. The kernels may also be called from C or Fortran, by manually wrapping the kernel calls in a C function. We plan to generate a C and Fortran interface automatically in the future.

5 APPLICATION TO AN ADER-DG METHOD

We integrated YATeTo in two codes in order to evaluate practicability of our design, as well as to evaluate the performance and optimisation opportunities. Both codes employ a discontinuous Galerkin method with ADER time-stepping based on the discrete Cauchy-Kovalewski procedure [Käser et al. 2007]. Furthermore, both codes solve a linear PDE in two or three dimensions of the form of Equation (2). The differences lie in the PDE (elastic wave equation, acoustic wave equation) and the underlying finite elements (tetrahedra, rectangles).

In the following, we do not derive the numerical schemes but only indicate changes w.r.t. literature references, in order to stay within the scope of this paper. We validated both codes with a plane wave problem (e.g. [Käser et al. 2007]), and checked that the code converges (for an appropriately chosen time-step) and that the observed convergence order matches the theoretical order of the scheme. Moreover, we tried to keep the amount of indices to a minimum by mostly omitting dependencies on space and time. We use the Einstein convention for subscript indices, but not for superscript indices.

5.1 SeisSol

The earthquake simulation code SeisSol (www.github.com/SeisSol/SeisSol) solves the seismic wave equation with support for elastic [Dumbser and Käser 2006], viscoelastic [Käser et al. 2007], and viscoplastic rheological models [Wollherr et al. 2018]. The code operates on unstructured tetrahedral meshes and the quantities are approximated with Dubiner’s basis functions. In essence, one may write the computational kernels as matrix chain products of small matrices, where small means that the maximum dimension size of each matrix is smaller or equal $\mathcal{B} = \binom{N+3}{3}$, where N is the maximum polynomial degree of the basis functions and $\mathcal{O} = N + 1$ is the theoretical convergence order. SeisSol already makes use of the code generator tailored for matrix chain products, which simplifies the implementation of the various rheological models [Uphoff and Bader 2016].

For elastic rheological models, the code achieves about 50 % of peak performance on compute clusters based on Intel’s Haswell or Knight’s Landing architecture [Heinecke et al. 2016a; Uphoff et al. 2017]. Moreover, the authors of [Breuer et al. 2017] investigate the possibility to fuse multiple simulations in a single run, using the same ADER-DG method as SeisSol and an elastic rheological model. They report a speed-up of $2.1\times$ for a fourth-order scheme, when fusing 8 simulations in one run (compared to 8 individual simulations). Their main optimisation ingredient is a specialised code generator for tensor contractions involving 3D tensors and sparse matrices.

5.1.1 ADER-DG. The numerical scheme of SeisSol is given in detail in [Dumbser and Käser 2006; Käser et al. 2007; Uphoff et al. 2017], and is stated in a compact form in Equations (13) to (16) for an elastic rheological model. The equations already include multiple simulations, as in [Breuer et al. 2017]. Multiple simulations are easily modelled using the Einstein convention as one simply has to add another index to the degrees of freedom, which we have denoted with a blue s .

The first step in the numerical scheme is to compute the time-derivatives of the degrees of freedom Q , using a Cauchy-Kovalewski procedure:

$$\mathcal{D}_{skp}^{(\delta+1)} := \tilde{K}_{kl}^{\xi} \mathcal{D}_{slq}^{\delta} A_{pq}^* + \tilde{K}_{kl}^{\eta} \mathcal{D}_{slq}^{\delta} B_{pq}^* + \tilde{K}_{kl}^{\zeta} \mathcal{D}_{slq}^{\delta} C_{pq}^*, \text{ where } \mathcal{D}_{skp}^0 := Q_{skp}^{\mu\tau}. \quad (13)$$

The indices μ and τ denote the space-time element and index δ denotes the order of the time-derivative. The matrices \tilde{K} are sparse $\mathcal{B} \times \mathcal{B}$ matrices, and A^* , B^* , and C^* are sparse 9×9 matrices, which are element-dependent linear combinations of the Jacobians A , B , and C from Equation (2). For every simulation one needs to store a $\mathcal{B} \times 9$ matrix for the degrees of freedom Q and the derivatives \mathcal{D} , yielding $\mathcal{S} \times \mathcal{B} \times 9$ tensors, where \mathcal{S} is the number of simulations.

The evolution in time is predicted with a Taylor expansion, without considering an element's boundaries. In the DG-scheme, the time-integral over a time-step with size Δt is required, which is computed as

$$\mathcal{I}_{skp} := \sum_{\delta=0}^N \frac{\Delta t^{\delta+1}}{(\delta+1)!} \mathcal{D}_{skp}^{\delta}. \quad (14)$$

The time-integral is inserted into the DG-scheme, yielding the update scheme for the degrees of freedom.

$$Q_{skp}^{\mu(\tau+1)} := Q_{skp}^{\mu\tau} + \hat{K}_{kl}^{\xi} \mathcal{I}_{slq} A_{pq}^* + \hat{K}_{kl}^{\eta} \mathcal{I}_{slq} B_{pq}^* + \hat{K}_{kl}^{\zeta} \mathcal{I}_{slq} C_{pq}^* + \sum_{\sigma=1}^4 \hat{R}_{km}^{\sigma} \tilde{R}_{lm}^{\sigma} \mathcal{I}_{slq} (A^+)_{pq}^{\sigma} + \quad (15)$$

$$+ \sum_{\sigma=1}^4 \hat{R}_{km}^{\sigma} f_{mn}^{\text{Rot}(\sigma, \mu)} R_{ln}^{\text{Face}(\sigma, \mu)} \mathcal{I}_{slq}^{\text{Neigh}(\sigma, \mu)} (A^-)_{pq}^{\sigma}. \quad (16)$$

The matrices \hat{K} are sparse $\mathcal{B} \times \mathcal{B}$ matrices, \hat{R} , \tilde{R} , and R are sparse $\mathcal{B} \times \tilde{\mathcal{B}}$ matrices, where $\tilde{\mathcal{B}} = \binom{N+2}{2}$, and f are sparse $\tilde{\mathcal{B}} \times \tilde{\mathcal{B}}$ matrices. A^+ and A^- contain the solution to the 1D Riemann problem which is solved along the four sides of a tetrahedron, and these are dense 9×9 matrices.

5.1.2 Equivalent sparsity patterns. The matrices \hat{K} contain large zero blocks, especially only the first $\tilde{\mathcal{B}}$ columns are non-zero. YATeTo automatically determines that the EQSPP of \mathcal{I} is a $\mathcal{S} \times \tilde{\mathcal{B}} \times 9$ subtensor. Hence, the contraction $\mathcal{I}_{sl[q]} \hat{K}_{kl}^T$ is mapped to a GEMM of size $(M, N, K) = (\mathcal{S}, \mathcal{B}, \tilde{\mathcal{B}})$ instead of a GEMM of size $(\mathcal{S}, \mathcal{B}, \mathcal{B})$. Also the contraction $\mathcal{I}_{(sl)q} (A^*)_{pq}^T$ is automatically mapped to a GEMM of size $(\mathcal{S}\tilde{\mathcal{B}}, 9, 9)$ instead of a GEMM of size $(\mathcal{S}\mathcal{B}, 9, 9)$. So the percentage of original flops scales with $3/(N+3)$, e.g. 50% for a fourth-order scheme or 37.5% for a sixth-order scheme.

The sparsity pattern of \tilde{K} is equivalent to the sparsity pattern of \hat{K}^T and it has a staircase structure. The effect is, that derivative D^{δ} has only $\binom{N-\delta+3}{3}$ non-zero coefficients per quantity [Breuer et al. 2014b]. We may set the sparsity patterns of the derivatives D^{δ} accordingly in order to exploit the vanishing coefficient – or we use existing visitors of YATeTo in order to simultaneously define the derivative kernels and determine the sparsity patterns of the derivatives automatically, as shown in Figure 6.

5.1.3 Strength reduction. By solving the matrix chain multiplication order problem the number of required flops in Equation (16) can be reduced from $O(N^6)$ to $O(N^5)$ [Uphoff et al. 2017]. The optimal matrix chain order $\hat{R}_{ka} \left(\left(f_{ab} \left(R_{lb} \mathcal{I}_{lq} \right) \right) A_{pq}^- \right)$ is reproduced by the implementation of the strength reduction algorithm. Interestingly, for 8–32 fused simulations the order of evaluation $\left(\hat{R}_{ka} f_{ab} \right) \left(\left(R_{lb} \mathcal{I}_{lq} \right) A_{pq}^- \right)$ is optimal, found automatically by strength reduction.

5.1.4 Optimal index permutations. We take Equation (16) as example, but note that the same discussion can be applied to the other kernels. From YATeTo we obtain the following mappings to LoG for either a single simulation or for

```

D = [Q]
for i in range(1,order):
    derivativeSum = Add()
    for j in range(3):
        derivativeSum += db.kDivMT[j]['k1'] * D[-1]['slq'] * db.star[j]['qp']
    derivativeSum = DeduceIndices( D[-1]['skp'].indices ).visit(derivativeSum)
    derivativeSum = EquivalentSparsityPattern().visit(derivativeSum)
    dQ = Tensor('dQ({})'.format(i), qShape, spp=derivativeSum.eqsp())
    g.add('derivative({})'.format(i), dQ['skp'] <= derivativeSum)
    D.append(dQ)

```

Fig. 6. Exemplary code which models vanishing coefficients in the Cauchy-Kovalevski procedure from Equation (13). First a partial AST is built and stored in `derivativeSum`. Then the first two visitors in the transformation process shown in Figure 1 are used to obtain the sparsity pattern of derivative D^i . Finally, a tensor using the derived sparsity pattern is defined and a complete AST is added to the code generator.

multiple simulations (Greek letters denote temporary tensors):

| Single | Multiple |
|---|--|
| $\alpha_{nq} := R_{ln}^T I_{lq}$ | $\alpha_{sn[q]} := I_{sl[q]} R_{ln}$ |
| $\beta_{mq} := f_{mn} \alpha_{nq}$ | $\beta_{(sn)p} := \alpha_{(sn)q} (A^-)_{pq}^T$ |
| $\gamma_{mp} := \beta_{mq} (A^-)_{pq}^T$ | $\gamma_{kn} := \hat{R}_{km} f_{mn}$ |
| $Q_{kp} := Q_{kp} + \hat{R}_{km} \gamma_{mp}$ | $Q_{sk[p]} := Q_{sk[p]} + \beta_{sn[p]} \gamma_{kn}^T$ |

We observe that the optimal index permutation algorithm from Section 4.5 fulfils the goals of the cost function: Non-unit stride GEMMs are not present, transposes are kept to a minimum and indices are fused if possible.

In SeisSol, the implementation is in fact a bit different: The A^- and R matrices (as well as the star matrices and the A^+ matrices) are stored transposed, such that a transpose-free scheme is obtained. For multiple simulations we can also obtain a transpose-free scheme in the following manner: The A^- matrices (as well the star matrices and the A^+ matrices) are stored transposed as for a single simulation, but for the other matrices we face the opposite situation: The R matrices are stored in normal order and we have to store \hat{R} and f transposed as well as \hat{K} and \tilde{K} for the other kernels.

5.1.5 Findings. YATeTo is able to reproduce the major optimisations from SeisSol: Zero-blocks are exploited and the optimal matrix chain multiplication order is found. For multiple simulations, zero blocks are also exploited automatically, strength reduction revealed the optimal—and different—evaluation order, and a transpose-free scheme is found by inspection of mappings to GEMM produced by YATeTo.

5.2 LinA

The code LinA was developed for education purposes, and contains a basic implementation of the ADER-DG method. LinA solves the linearised equations of acoustics in two dimensions [LeVeque 2002], which involve the three quantities pressure and particle velocities in horizontal and vertical direction. A uniform mesh with rectangular elements is used.

Our goal here is to evaluate the application of YATeTo to a DG-spectral-element-like method (cf. [Kopriva 2009, Chapter 5.4] for an introduction to DG-SEM). As briefly introduced in Section 3, quantities are represented using a tensor product basis, i.e. $q_p = Q_{lmnp} \psi_l(x) \psi_m(y) \psi_n(z)$. An advantage of DG-SEM is that integrals over the reference elements may be split in a tensor product of 1D integrals. E.g. the computation of the gradient in the weak form can

be done with $O(N^{d+1})$ instead of $O(N^{2d})$ computations per element, where d is the number of dimensions. On the downside, one needs to store $(N+1)^d$ degrees of freedom per quantity instead of $\binom{N+d}{d}$ per quantity, which is the minimum amount of degrees of freedom needed to represent the same space of polynomials.

We implemented the ADER-DG-SEM method in LinA using YATeTo (www.github.com/TUM-15/LinA), and extended the code to three dimensions, which implies an additional quantity or 4 quantities in total. For the 1D basis functions ψ_i we use a nodal basis with Gauss-Lobatto points and Legendre polynomials [Hesthaven and Warburton 2008]. In the following we are going to abuse notation and use the same symbols for tensors as in SeisSol, even though the tensors are of different shape and have different sparsity patterns.

5.2.1 Numerical scheme. The first step in LinA, as in SeisSol, is to predict the element-local evolution in time:

$$\mathcal{D}_{xyzp}^{(\delta+1)} := \tilde{K}_{xl} \mathcal{D}_{lyzq}^\delta A_{pq}^* + \tilde{K}_{ym} \mathcal{D}_{xmzq}^\delta B_{pq}^* + \tilde{K}_{zn} \mathcal{D}_{xynq}^\delta C_{pq}^*, \text{ where } \mathcal{D}_{xyzp}^0 := Q_{xyzp}^{\xi v \zeta \tau}, \quad (17)$$

$$\mathcal{I}_{xyzp} := \sum_{\delta=0}^N \frac{\Delta t^{\delta+1}}{(\delta+1)!} \mathcal{D}_{xyzp}^\delta, \quad (18)$$

Indices ξ, v, ζ denote the location of an element on the grid and τ is the time index. The matrices \tilde{K} are $(N+1) \times (N+1)$ matrices and A^* and B^* are sparse 4×4 matrices. Both Q and \mathcal{D} are $(N+1) \times (N+1) \times (N+1) \times 4$ tensors.

The weak derivatives are evaluated afterwards:

$$Q_{xyzp}^* := Q_{xyzp}^{\xi v \zeta \tau} + \hat{K}_{xl} \mathcal{I}_{lyzq} A_{pq}^* + \hat{K}_{ym} \mathcal{I}_{xmzq} B_{pq}^* + \hat{K}_{zn} \mathcal{I}_{xynq} C_{pq}^* \quad (19)$$

In contrast to SeisSol, the neighbour exchange is not based on volume data. Instead, it is sufficient to consider the boundary nodes. We copy the boundary nodes to continuous storage for each side, such that we need to store eight 3D tensors instead of a single 4D tensor. In YATeTo, we represent the ‘‘copy’’ operation by the following matrix-vector products:

$$\mathcal{X}_{yzp}^\sigma := F_l^\sigma \mathcal{I}_{lyzq}, \quad \mathcal{Y}_{xzp}^\sigma := F_m^\sigma \mathcal{I}_{xmzq}, \quad \mathcal{Z}_{xyp}^\sigma := F_n^\sigma \mathcal{I}_{xynq}, \quad (20)$$

where $F_i^\sigma = \delta_{i0}$ for $\sigma \in \{\text{left, bottom, back}\}$, and $F_i^1 = \delta_{iN}$ for $\sigma \in \{\text{right, top, front}\}$. The 2D boundary nodes are then used to apply the numerical fluxes:

$$\begin{aligned} Q_{xyzp}^{\xi v \zeta (\tau+1)} := & Q_{xyzp}^* + \sum_{\sigma \in \{\text{left, right}\}} \hat{F}_x^\sigma \left(\mathcal{X}_{yzq}^\sigma (A^+)_{pq}^\sigma + \mathcal{X}_{yzq}^{\text{Neigh}(\sigma, \xi, v, \zeta)} (A^-)_{pq}^\sigma \right) + \\ & + \sum_{\sigma \in \{\text{bottom, top}\}} \hat{F}_y^\sigma \left(\mathcal{Y}_{xzq}^\sigma (A^+)_{pq}^\sigma + \mathcal{Y}_{xzq}^{\text{Neigh}(\sigma, \xi, v, \zeta)} (A^-)_{pq}^\sigma \right) + \\ & + \sum_{\sigma \in \{\text{back, front}\}} \hat{F}_z^\sigma \left(\mathcal{Z}_{xyq}^\sigma (A^+)_{pq}^\sigma + \mathcal{Z}_{xyq}^{\text{Neigh}(\sigma, \xi, v, \zeta)} (A^-)_{pq}^\sigma \right) \quad (21) \end{aligned}$$

5.2.2 Implementation. Mapping the numerical scheme to our DSL is simple as one may almost copy the above formulation in Einstein notation. E.g. the last line in Equation (21) can be written as following:

```
Q['xyzp'] <= Q['xyzp'] + Fhat[side]['z'] * \
(Z['xyq'] * Aplus['pq'] + ZNeigh['xyq'] * Aminus['pq'])
```

Furthermore, by inspecting the generated implementation we decided to store the matrices A^*, B^*, C^*, A^+, A^- transposed and also a transposed copy of \hat{K} and \tilde{K} , which leads to a transpose-free scheme. The eventual C++-code for the last line in Equation (21) can be seen in Figure 7. There, a generic nested loop-code implements the outer product

```

void kernel::flux::execute2() {
  assert(FDivM(0) != nullptr);
  assert(Q != nullptr);
  assert(Q1 != nullptr);
  assert(Q1Neighbour != nullptr);
  assert(fluxSolver != nullptr);
  assert(fluxSolverNeighbour != nullptr);
  double *_tmp0;
  double _buffer0[1024] __attribute__((aligned(64)));
  _tmp0 = _buffer0;
  pspamm_m256_n4_k4_ldA256_ldB4_ldC256_alpha1_beta0_alignedA1_alignedC1_pfsigonly(
    Q1, fluxSolver, _tmp0, 1, 0, nullptr
  );
  pspamm_m256_n4_k4_ldA256_ldB4_ldC256_alpha1_beta1_alignedA1_alignedC1_pfsigonly(
    Q1Neighbour, fluxSolverNeighbour, _tmp0, 1, 1, nullptr
  );
  for (int p = 0; p < 4; ++p)
    for (int z = 0; z < 16; ++z)
      for (int y = 0; y < 16; ++y) {
        #pragma omp simd
        for (int x = 0; x < 16; ++x) {
          Q[1*x + 16*y + 256*z + 4096*p] += FDivM(0)[1*z] * _tmp0[1*x + 16*y + 256*p];
        }
      }
}

```

Fig. 7. Sample C++-code generated in LinA. Indices in tensor contractions are fused such that only a call to GEMM is required. The GEMMs (prefix pspamm) are separate functions which contain inline assembler code, and are generated specifically for the kernel. The nested loops implement an outer product, and were generated using the generic fallback code generator.

$Q_{xyzp} := \text{tmp}_{xy} \hat{F}_z + Q_{xyzp}$. In principle, one might also map this operation to BLAS, e.g. in terms of the level 2 routine GER, which implements a rank-1 update of a matrix. That is, one could implement the outer product as a Loop-over-GER, i.e. $Q_{(xy)z[p]} := \text{tmp}_{(xy)[p]} \hat{F}_z + Q_{(xy)z[p]}$. In YATeTo such an implementation corresponds to adding another back-end. However, we leave the implementation and performance evaluation of Loop-over-GER for future work.

6 IMPLEMENTATION ASPECTS AND PERFORMANCE RESULTS

In this section we thoroughly evaluate the performance of the applications presented in Section 5. From the results in this section we ultimately want to answer the following questions: First, is our tensor toolbox able to reproduce SeisSol’s performance for the special case of matrix chain products? Second, can we achieve similar performance improvements as in [Breuer et al. 2017] by fusing multiple simulations, but using our generic approach? Third, do we still get high performance when changing the PDE, the finite element type, and the basis functions?

6.1 Hardware and software environment

We run all our performance tests on two recent Intel architectures:

KNL Intel Xeon Phi 7250 on Stampede 2, “Knights Landing”, single socket configuration with 68 cores, 1.4 GHz nominal frequency, 1.6 GHz single-core turbo frequency, theoretical peak performance of 3.0 TFLOPS using

double precision or 6.1 TFLOPS using single precision (at 1.4 GHz), 1 MiB private L2 cache per tile (shared between two cores).

SKX Intel Xeon Platinum 8174 on SuperMUC-NG, “Skylake”, dual socket configuration with 24 cores per socket, 3.1 GHz nominal frequency, 2.7 GHz AVX-512 all-core turbo frequency,⁶ theoretical peak performance of 4.1 TFLOPS using double precision or 8.3 TFLOPS using single precision, 1 MiB private L2 cache per core, 1.375 MiB shared L3 cache per core (non-inclusive).

In each experiment, threads are pinned to cores using the `KMP_AFFINITY` or `OMP_PLACES` environment variable. On SKX we use 48 threads and pin each thread to exactly one core. For simultaneous multithreading (SMT) we use a compact pinning with 2 threads per core. On KNL we basically employ the same strategy with a maximum of 2 threads per core, but we leave the first tile free for the operating system. Thus we use 66 threads without SMT and 132 threads with SMT. Furthermore, on KNL we use the cache memory mode for SeisSol and the flat memory mode for LinA, where memory is bound to MCDRAM using `numactl`.

Our software is compiled with the Intel C++-compiler (version 18). We generate our GEMM kernels with LIBXSMM (version 1.10, [Heinecke et al. 2016b]) and PSpaMM (commit f59f98d, [Wauligmann and Brei 2019]), which both offer highly tuned GEMMs for KNL and SKX. LIBXSMM is used in static mode (instead of the just-in-time-compilation mode), i.e. code is generated at compile-time. We remark that the generated file `subroutine.cpp`, which contains kernels from LIBXSMM and PSpaMM, is compiled with option `-mno-red-zone`. Otherwise, the compiled code might be wrong due to a combination of (1) the compiler does not inspect inline assembly, (2) the generated code might modify the stack (`pushq`, `popq`), (3) Linux calling conventions.

If not stated otherwise, we report the minimum run-time over at least 5 runs.

6.2 Sparse matrices

PSpaMM originated from a student research project for dense \times sparse matrix multiplications [Brei 2018]. The starting point of the project is a clone of the almost optimal register-blocked LIBXSMM kernels for KNL. In principle, sparse matrix multiplication is then implemented by removing every instruction that either is a multiplication with zero or becomes unnecessary (such as loads of never used data). Control structures such as the row indices array and the column pointer array are completely unrolled.

An issue with unrolling control structures is that code is also data, which needs to be fetched from memory or cache. An experiment with random sparse matrices in [Brei 2018], using a predecessor of PSpaMM, suggests that the generated dense \times sparse matrix multiplication is always faster than its dense \times dense counterpart—as long as the number of non-zeros stays below a threshold such that code stays in the L1i cache. The threshold can be estimated by dividing the L1i cache size by the size of a fused multiply-add instruction, as a fused multiply-add instruction is generated for every non-zero in the sparse matrix.

The sparse \times dense case is more involved [Breuer et al. 2014a], the fundamental issue being that the standard outer product formulation for matrix multiplications forces to vectorise over sparse vectors. In SeisSol, sparse \times dense kernels did not improve time-to-solution on KNL [Heinecke et al. 2016a].

⁶We could not find a processor specification as the 8174 is a special model. The system’s peak performance is claimed to be 26.3 PFLOPS on 6336 nodes (<https://doku.lrz.de/display/PUBLIC/Hardware+of+SuperMUC-NG>), which would imply a peak AVX-512 frequency of 2.7 GHz. A test measuring the time of around 54 billion `vfmadd231pd` instructions (using alternating `zmm` registers) indicates that a peak frequency of 2.79 GHz is possible. In this paper we adopt the vendor’s claim of 2.7 GHz, but we encourage the reader to scale the results with a peak frequency that may be more appropriate.

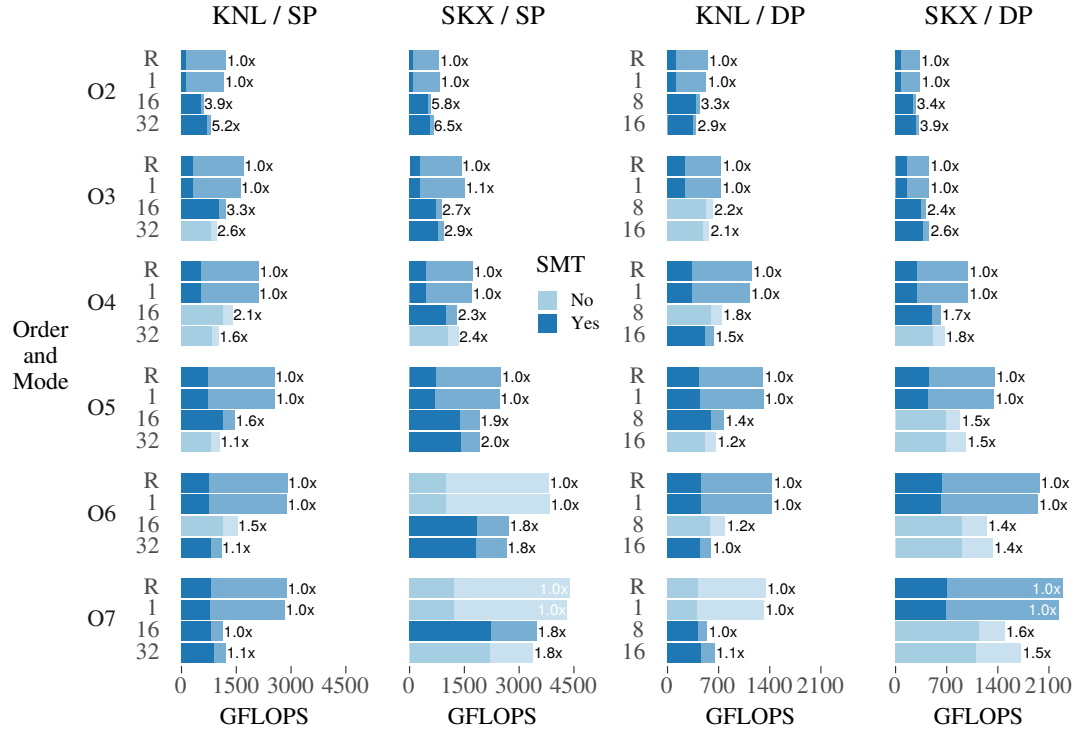


Fig. 8. The figure shows performance experiments with SeisSol’s kernels. We compare architectures (KNL, SKX), precision (SP=single, DP=double), orders (O2–O7), and the number of simultaneous simulations (1–32). The letter R (reference) denotes the latest SeisSol release [Uphoff et al. 2017]. Dark bars show non-zero flops and light bars denote hardware flops and the shade of blue indicates if SMT increases performance. Numbers right to bars show speed-ups, if one compares S simultaneous simulations to S individual simulations. The benchmark results are tabulated in Appendix A.

As a consequence, we employ the following rule: We use a sparse memory layout when a sparse matrix is multiplied from the right and we use a dense memory layout when a sparse matrix is multiplied from the left.

6.3 SeisSol: Performance

In this section, we present and discuss the performance results for SeisSol shown in Figure 8. We note that SeisSol’s performance reproducer is used [Uphoff et al. 2017]. The latter calls the same kernels as SeisSol does, but the reproducer operates on random initial data and the cell neighbouring relations are random.

We investigate single precision arithmetic as well as double precision arithmetic. (As YATeTo supports single and double precision, we take an agnostic viewpoint on necessary precision and simply generate and test both precisions.) Furthermore, we ran the performance reproducer of the latest SeisSol release for reference [Uphoff et al. 2017]. Performance is measured in terms of non-zero flops and hardware flops. The important measure here is non-zero flops, as it is independent of the choice of sparse and dense memory layouts and as such represents time-to-solution. However, the non-zero flops measure assumes perfect usage of sparsity patterns and we see it as too optimistic w.r.t. hardware. Hence we include hardware flops as measure of exploitation of the hardware’s capabilities.

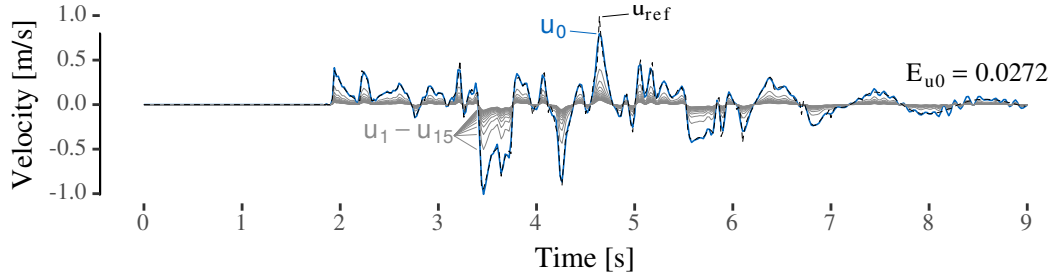


Fig. 9. Comparison of simulation and reference solution. Shown is the particle velocity in x-direction of the 9-th receiver of the LOH.1 benchmark (see http://www.sismowine.org/model/WP2_LOH1.pdf). A total of 16 simulations ran simultaneously in single precision, where the 0-th simulation has the same seismic moment as the reference. Other simulations (u_1-u_{15}) have a reduced moment (see text). The relative seismic moment misfit for the 0-th simulation is shown in E_{u0} .

Table 1. Summary of performance results for the LOH.1 benchmark using 8 SKX nodes and O6.

| Precision | LTS | Mode | NZ-GFLOPS | HW-GFLOPS | % HW _{proxy} | Time / Sim. [min] |
|-----------|-----|------|-----------|-----------|-----------------------|-------------------|
| DP | No | 1 | 524 | 1618 | 83 | 42.1 |
| DP | No | 8 | 839 | 1148 | 92 | 26.6 |
| DP | Yes | 1 | 480 | 1485 | 76 | 17.8 |
| DP | Yes | 8 | 752 | 1030 | 83 | 11.5 |
| SP | No | 1 | 840 | 3217 | 84 | 26.2 |
| SP | No | 16 | 1719 | 2559 | 94 | 13.0 |
| SP | Yes | 1 | 789 | 3023 | 79 | 10.8 |
| SP | Yes | 16 | 1433 | 2134 | 78 | 6.0 |

In Figure 8 we observe that the results for single simulations (row “1”) closely match the performance of the reference (row “R”) over all orders, architectures, and precisions. We conclude that the special case of matrix chain multiplications is well handled within YATeTo. We also see that there is a large gap between non-zero flops and hardware flops. The latter is due to handling sparse matrices as dense, which minimises time-to-solution according to an auto-tuning procedure [Heinecke et al. 2016a]. For multiple simulations (rows “8”, “16”, and “32”), most sparse matrices are multiplied from the right such that the favourable dense \times sparse case is obtained. Moreover, the arithmetic intensity is higher as matrices already in cache are reused [Breuer et al. 2017]. In our experiments, we observe that multiple simulations (compared to the same amount of individual simulations) yield a speed-up of $1.1\times-3.9\times$ for DP and $1.1\times-6.5\times$ for SP. Furthermore, we observe an increase in non-zero peak performance from $1.1\%-16.9\%$ to $6.7\%-27.5\%$. Specifically, a non-zero peak efficiency of 19.6% for KNL O4 DP is obtained, which is within a few percent of the non-zero peak efficiency obtained in [Breuer et al. 2017].⁷

6.4 SeisSol: Validation

In Section 6.3 a performance reproducer is used to evaluate SeisSol’s performance. Here, we evaluate the correctness of the implementation using the well-established Layer Over Halfspace 1 (LOH.1) benchmark [Day et al. 2003]. The model description as well as the reference solution is taken from the SeISmic MOdeling Web INterfacE (www.sismowine.org).

We ran a total of 8 or 16 simulations simultaneously on a mesh with 1.1 million elements and Order 6. The 0-th simulation has a seismic moment of $M_0 = 10^{18}$ Nm, as required by the benchmark. Other simulations have a seismic moment of $M_0/(1 + s)$ where s is the simulation number, i.e. $M_0/2$, $M_0/3$, $M_0/4$, etc. Due to the PDEs being linear, we expect that the amplitude of particle velocities is reduced by the same factor. Figure 9 shows that the 0-th simulation matches the reference well, with a low relative seismogram misfit. The other simulations have their amplitude reduced, as expected. We note that the relative seismogram misfit is identical up to 3 digits, independent of the number of simulations or floating point precision.

The measured performance on 8 SKX nodes is shown in Table 1, where we evaluated single simulations and multiple simulations, SP and DP, as well as Global Time Stepping (GTS) and Local Time Stepping (LTS). SMT is enabled or disabled according to Figure 8, but only 47 cores for computation are used as one core is left for a communication thread. We observe that we obtain a lower performance in comparison to the performance reproducer (see column % HW_{proxy}). We do not attempt a detailed comparison of the performance reproducer with the real application, however, it is interesting to note that for multiple simulations we “lose” less performance than for a single simulation (e.g. 84 % vs. 94 % for GTS-SP). The latter is a hint that the remaining serial part of SeisSol might be responsible for the lower performance, as the serial part is mostly independent of the number of simulations but the parallel part becomes more expensive for more simulations. LTS is less efficient due to smaller loop lengths, but pays off in time-to-solution. In total, the expected speed-up of multiple simulations is reproduced (1.6× for GTS-DP, 2.0× for GTS-SP).

6.5 LinA

While LinA uses the same ADER-DG scheme as SeisSol, the implementation is very different due to the use of tensor basis functions and cuboid elements. The main difference is that the arithmetic intensity only grows linear with polynomial degree, instead of cubic growth as in SeisSol. But due to the use of a nodal basis, most of the matrices in the scheme are dense or almost dense and sparsity mainly comes in due to the coefficient matrices of the PDE. Another issue is the increased storage required by the degrees of freedom, such that the last level cache size is becoming an issue for three spatial dimensions, hence we also tested the scheme in two spatial dimensions to better understand the tradeoff between arithmetic intensity and cache usage.

A general observation in the performance results shown in Figure 10 is that we require at least order 16 in order to surpass the 1 TFLOPS mark in double precision (or equivalently 2 TFLOPS in single precision), which is in SeisSol already passed for order 5. This mark is surpassed in 2D for all orders except 8, but in 3D only on SKX for orders 16 and 24 in double precision and orders 16 and 32 in single precision. The reason for the observed behaviour becomes clear when considering cache usage in the ADER kernel (Equations (17) and (18)), which contains the major part of the computational load per element: Inside ADER we require storage for four tensors of size $O^d(1 + d)$, where $O = N + 1$ is the order of the scheme and d is the number of spatial dimensions. We need one buffer for the current and the next derivative, one buffer contains the time integral, and another temporary buffer is used for intermediate products. In 2D, a maximum storage size of 96 KiB is required for all four tensors, which easily fits into L2 caches. In 3D, we require

⁷We note that the schemes of [Uphoff et al. 2017] and [Breuer et al. 2017] are not identical due to a different handling of the boundary integral terms, however the remainder of the scheme is identical.

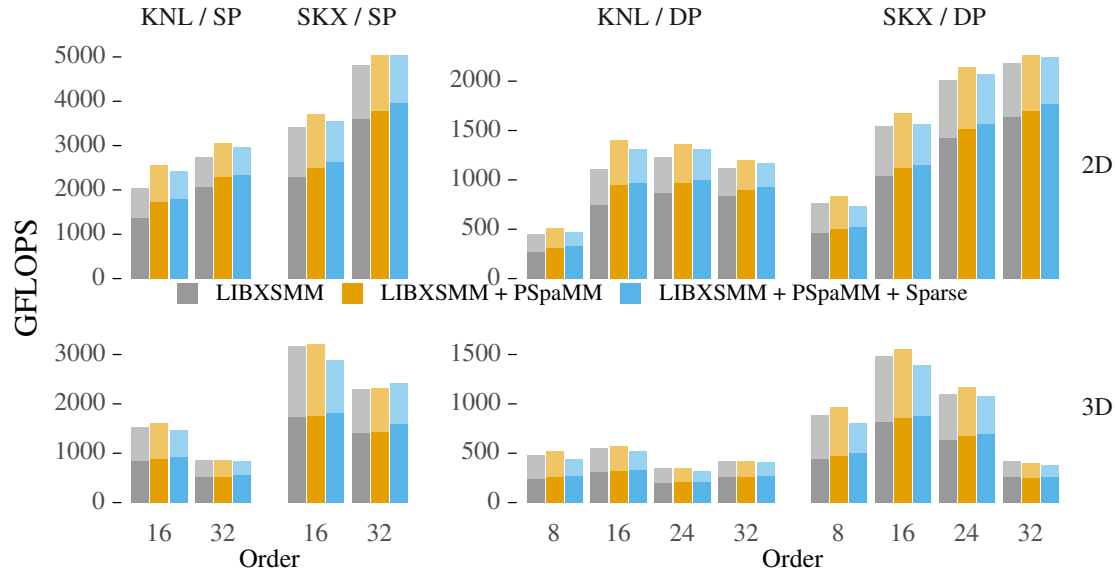


Fig. 10. We show performance results of a DG-SEM method implemented in the code LinA. We compare architectures (KNL, SKX), precision (SP=single, DP=double), orders (8, 16, 24, 32), and number of spatial dimensions (2D, 3D). Dark bars show non-zero flops and light bars denote hardware flops. The colour indicates the employed code generators as well as the usage of the CSC memory layout for some matrices.

512 KiB, 1.7 MiB, and 4 MiB for orders 16, 24, and 32, and half the amount for single precision respectively. So on KNL we need the full L2 cache per core for the four tensors when using double precision, hence necessary cache lines are evicted from L2 cache during ADER and we get a low arithmetic intensity. As we only need 256 KiB for order 16 in single precision, the latter discussion also explains why O16 SP is more than $2\times$ faster than O16 DP. On SKX we have a total of 2.1375 MiB cache per core, as the L3 cache is non-inclusive. Thus, only for O32 DP tensors are evicted from cache.

Moreover, we obtain an additional performance boost due to the choice of code generator and memory layout. For the evaluation of the flux function (i.e. multiplication with A^* , B^* , and C^*) we have to contract the degrees of freedom with matrices smaller than $(d+1) \times (d+1)$. We performed micro-benchmarks on KNL which suggest that the LIBXSMM kernels are sub-optimal for such matrix sizes, which we believe to be due to superfluous `vaddpd` instructions and due to the fixed $8 \times N$ register blocking on KNL. As a consequence, we added PSpaMM to replace the sub-optimal kernels, which is implemented in YATeTo by specifying a list of code generators, where we may give higher preference to a code generator for specific matrix sizes. Using PSpaMM and LIBXSMM combined gives us a non-zero performance boost up to 202 GFLOPS in DP or up to 344 GFLOPS in SP (for KNL O16 in 2D). Using a CSC memory layout for the matrices A^* , B^* , and C^* gives a further performance boost up to 74 GFLOPS in DP or up to 194 GFLOPS in SP (for SKX O32 in 2D). In total we obtain a performance increase of up to 31% for DP and 30% for SP, and a maximum non-zero peak performance of 1769 GFLOPS for DP and 3969 GFLOPS for SP.

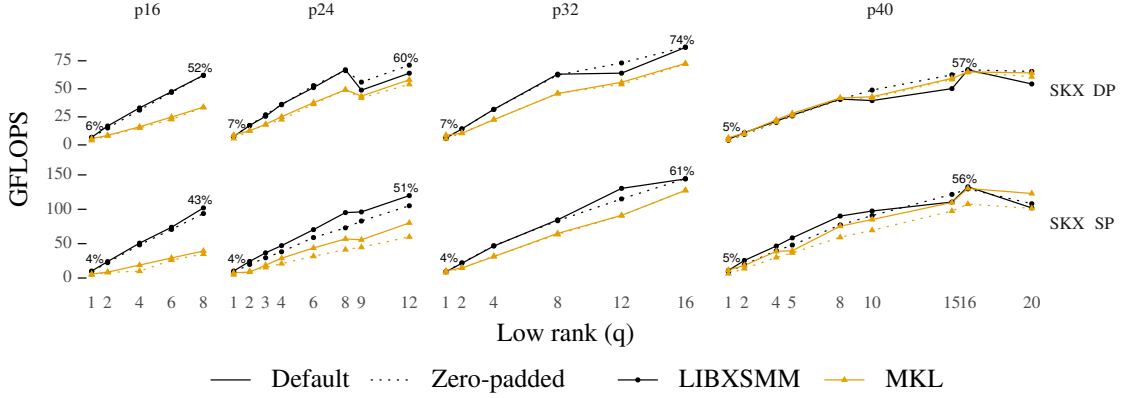


Fig. 11. Performance of the kernel from Equation (22) for multiple tensor sizes p and q (see text). The plot shows non-zero flops, i.e. artificial flops due to zero-padding are not counted. The single-core AVX-512 peak performance on SKX is calculated w.r.t. the empirically determined peak frequency of 3.7 GHz.

6.6 Findings

In this section we found that kernels generated with YATeTo are able to match the performance of [Uphoff et al. 2017] and all major optimisations of SeisSol are found automatically. The extension to multiple simulations closely matches the performance of [Breuer et al. 2017].

For LinA we saw that YATeTo does not save the developer from basic arithmetic intensity considerations, but high performance may be achieved with automatically generated kernels in the case of a large enough arithmetic intensity. Moreover, YATeTo’s ability to mix and match different code generators increased performance by up to 31 %.

7 ANOTHER AREA OF APPLICATION

Small tensor contractions are found to be the core of MADNESS [Stock et al. 2011], which is a framework for solving problems in quantum chemistry and other applications [Harrison et al. 2016]. Kernels in MADNESS often take the following form [Stock et al. 2011]:

$$R_{ijk} = S_{xyz} X_{xl}^L X_{li}^R Y_{ym}^L Y_{mj}^R Z_{zn}^L Z_{nk}^R \quad (22)$$

Each L-R matrix pair is obtained by a low-rank decomposition of a $p \times p$ matrix. In the following we assume that the low-rank is equal among all L-R pairs and given by q , such that indices l, m, n have size q and indices i, j, k, x, y, z have size p . The authors of [Stock et al. 2011] developed a code generator for such tensor contractions, which uses loop transformations and outputs loop-code and SSE3 intrinsics. In the following we investigate the performance of the above kernel when implemented with YATeTo.

The above expression is a natural fit for YATeTo’s DSL. We note that the optimal order of evaluation, as stated in [Stock et al. 2011], is found automatically. A few tweaks may be applied to the above formulation: First of all, the matrices X^L and X^R are stored already transposed, as then a transpose-free kernel is obtained. (The authors of [Stock et al. 2011] also store Z^L transposed.) Second, the rows of X^L and X^R may be padded with zeros, such that the number of rows are a multiple of the vector width (i.e. 8 in double precision and 16 in single precision.)

Figure 11 shows our performance results. We observe that in the extreme case of $q = 1$ we obtain low performance of 6.4 GFLOPS–8.8 GFLOPS in DP and 10.2 GFLOPS–11.6 GFLOPS in SP. A similar performance was achieved in [Stock et al. 2011] for $q = 1$, even though they used a CPU from the year 2008. A potential issue is that the generated GEMMs degenerate to either inner products, outer products, or scalar multiplications. Moving to larger values of q , we see a steady increase in performance, up to 87.3 GFLOPS in DP and 144.6 GFLOPS in SP, which corresponds to 74 % and 61 % of the theoretical peak performance w.r.t. the empirically determined AVX-512 peak frequency of 3.7 GHz, respectively.

Comparing LIBXSMM to MKL we see that using LIBXSMM is beneficial in most cases, especially for small tensor sizes. In many cases zero-padding is either beneficial or delivers almost the same performance as its counterpart. But for cases p24 SP and p40 SP zero-padding mostly lowers performance. The reason for this behaviour stems likely from the multiplication with X^R : Here, the introduction of zeros leads to a non-fused GEMM, which is fused in the non-padded variant.

In summary, we find that mapping operations to GEMM might be sub-optimal for very small tensor contractions. However, given large enough tensor contractions we obtain high performance with low implementation effort, as the DSL naturally suits the problem description and the evaluation order with minimum cost is found automatically. Furthermore, the choice of memory layout (padded, non-padded) and GEMM back-end (LIBXSMM, MKL) might have a large impact on performance.

The example presented here is included in YATeTo’s main repository in the `examples` folder.

8 CONCLUSION AND OUTLOOK

We presented YATeTo, a tensor toolbox especially suited for small tensor operations. The toolbox includes standard techniques, such as strength reduction or the mapping of tensor operations to Loop-over-GEMM. To our best knowledge, we present novel optimisations for tensor operations such as equivalent sparsity patterns or optimal index permutations.

We included YATeTo in SeisSol, which allows to generate kernels for single forward simulations but also multiple forward simulations. From our point of view, the DSL simplifies the simultaneous implementation of single and multiple simulations considerably, but still allows to tune both implementation variants individually. Moreover, we integrated YATeTo in the tensor product based code LinA with low implementation effort.

The performance of our new SeisSol version matches its previous performance for a single simulation. For multiple simulations, we obtain speed-ups of $1.1\times$ to $6.5\times$ and a non-zero peak efficiency of up to 27.5 % on Skylake. In LinA, we saw that ability to mix-and-match GEMM kernels allows to increase performance by up to 31 %, leading to a non-zero peak efficiency of up to 48 %. Application of YATeTo to a literature example showed high performance over 50 % peak for large enough tensors, but likely sub-optimal performance for very small tensors.

A current limitation of our approach is that the employed code-generators for small matrix multiplications do not support transpositions. In our test cases we are able to avoid transpositions, but this might not be the case for other applications. However, one may always use a BLAS implementation like MKL, which support transpositions, and it is a simple matter to include further code generators or libraries that offer GEMM.

In future work we want to evaluate YATeTo for more applications and further back-ends. Especially, we are interested in vectorisation over elements (also sometimes called patches) for hexahedral meshes, or in curvilinear elements. Furthermore, we think that a useful extension to YATeTo are tools that assist the user in the development process. For example, a tool could automatically generate roof-line models or could estimate the cache usage of a kernel.

ACKNOWLEDGMENTS

The work in this paper was supported by the Volkswagen Foundation (ASCETE – Advanced Simulation of Coupled Earthquake-Tsunami Events, grant no. 88479). Computing resources were provided by the Intel Parallel Computing Center ExScaMIC-KNL and by the Leibniz Supercomputing Centre (project pr45fi).

REFERENCES

- H. L. Atkins and C.-W. Shu. 1998. Quadrature-Free Implementation of Discontinuous Galerkin Method for Hyperbolic Equations. *AIAA Journal* 36:5 (1998), 775–782.
- G. Baumgartner, A. Auer, D. E. Bernholdt, A. Bibireata, V. Choppella, D. Cociorva, X. Gao, R. J. Harrison, S. Hirata, S. Krishnamoorthy, S. Krishnan, C. chung Lam, Q. Lu, M. Nooijen, R. M. Pitzer, J. Ramanujam, P. Sadayappan, and A. Sibiryakov. 2005. Synthesis of High-Performance Parallel Programs for a Class of ab Initio Quantum Chemistry Models. *Proc. IEEE* 93, 2 (Feb 2005), 276–292.
- N. W. Brei. 2018. *Generating Small Sparse Matrix Multiplication Kernels for Knights Landing*. Master’s thesis. Technical University of Munich, Department of Informatics, Boltzmannstr. 3, 85748 Garching, Germany.
- A. Breuer, A. Heinecke, M. Bader, and C. Pelties. 2014a. Accelerating SeisSol by Generating Vectorized Code for Sparse Matrix Operators. In *Parallel Computing: Accelerating Computational Science and Engineering (CSE)*. IOS Press, 347–356.
- A. Breuer, A. Heinecke, and Y. Cui. 2017. EDGE: Extreme Scale Fused Seismic Simulations with the Discontinuous Galerkin Method. In *High Performance Computing, ISC 2017*. Springer International Publishing, Cham, 41–60.
- A. Breuer, A. Heinecke, S. Rettenberger, M. Bader, A.-A. Gabriel, and C. Pelties. 2014b. Sustained Petascale Performance of Seismic Simulations with SeisSol on SuperMUC. In *Supercomputing: 29th International Conference, ISC 2014*. Springer, 1–18.
- E. Cohen. 1998. Structure Prediction and Computation of Sparse Matrix Products. *Journal of Combinatorial Optimization* 2, 4 (1998), 307–332.
- T. H. Cormen, C. E. Leiserson, R. L. Rivest, and C. Stein. 2009. *Introduction to Algorithms* (3rd ed.). The MIT Press.
- S. M. Day, J. Bielak, D. Dreger, S. Larsen, R. Graves, A. Pitarka, and K. B. Olsen. 2003. Tests of 3D elastodynamics codes: Final report for Lifelines program task 1A02. Pacific Earthquake Engineering Research Center. (Oct 2003).
- E. Di Napoli, D. Fabregat-Traver, G. Quintana-Ortí, and P. Bientinesi. 2014. Towards an efficient use of the BLAS library for multilinear tensor contractions. *Appl. Math. Comput.* 235 (2014), 454 – 468.
- M. Dumbser and M. Käser. 2006. An arbitrary high-order discontinuous Galerkin method for elastic waves on unstructured meshes – II. The three-dimensional isotropic case. *Geophysical Journal International* 167 (2006), 319–336.
- A. Einstein. 1916. Die Grundlage der allgemeinen Relativitätstheorie. *Annalen der Physik* 354, 7 (1916), 769–822.
- E. Gamma, R. Helm, R. Johnson, and J. Vlissides. 1995. *Design Patterns: Elements of Reusable Object-oriented Software*. Addison-Wesley Longman Publishing Co., Inc., Boston, MA, USA.
- K. Goto and R. A. van de Geijn. 2008. Anatomy of high-performance matrix multiplication. *ACM Trans. Math. Softw.* 34, 3 (2008), 12:1–12:25.
- R. Harrison, G. Beylkin, F. Bischoff, J. Calvin, G. Fann, J. Fosso-Tande, D. Galindo, J. Hammond, R. Hartman-Baker, J. Hill, J. Jia, J. Kottmann, M. Yvonne Ou, J. Pei, L. Ratcliff, M. Reuter, A. Richie-Halford, N. Romero, H. Sekino, W. Shelton, B. Sundahl, W. Thornton, E. Valeev, Á. Vázquez-Mayagoitia, N. Vence, T. Yanai, and Y. Yokoi. 2016. MADNESS: A Multiresolution, Adaptive Numerical Environment for Scientific Simulation. *SIAM Journal on Scientific Computing* 38, 5 (2016), S123–S142.
- A. Heinecke, A. Breuer, M. Bader, and P. Dubey. 2016a. High Order Seismic Simulations on the Intel Xeon Phi Processor (Knights Landing). In *High Performance Computing: 31st International Conference, ISC High Performance 2016, Frankfurt, Germany, June 19-23, 2016, Proceedings*. Springer, 343–362.
- A. Heinecke, G. Henry, M. Hutchinson, and H. Pabst. 2016b. LIBXSM: Accelerating Small Matrix Multiplications by Runtime Code Generation. In *Proceedings of the International Conference for High Performance Computing, Networking, Storage and Analysis (SC ’16)*. IEEE Press, Piscataway, NJ, USA, 84:1–84:11.
- J. S. Hesthaven and T. Warburton. 2008. *Nodal Discontinuous Galerkin Methods*. Springer, New York, USA.
- M. Hutchinson, A. Heinecke, H. Pabst, G. Henry, M. Parsani, and D. Keyes. 2016. Efficiency of High Order Spectral Element Methods on Petascale Architectures. In *High Performance Computing: 31st International Conference, ISC High Performance 2016*. Springer, 449–466.
- M. Käser, M. Dumbser, J. de la Puente, and H. Igel. 2007. An arbitrary high-order Discontinuous Galerkin method for elastic waves on unstructured meshes – III. Viscoelastic attenuation. *Geophysical Journal International* 168 (2007), 224–242.
- D. Kempf, R. Heß, S. Müthing, and P. Bastian. 2018. Automatic Code Generation for High-Performance Discontinuous Galerkin Methods on Modern Architectures. *arXiv e-prints* (Dec. 2018).
- D. A. Kopriva. 2009. *Implementing Spectral Methods for Partial Differential Equations: Algorithms for Scientists and Engineers* (1st ed.). Springer.
- C. C. Lam. 1999. *Performance optimization of a class of loops implementing multi-dimensional integrals*. Ph.D. Dissertation. Graduate School of The Ohio State University, UMI Company, 300 North Zeeb Road Ann Arbor, MI 48103.
- C.-C. Lam, P. Sadayappan, C. Daniel, M. Alouani, and J. Wilkins. 1999. Performance Optimization of a Class of Loops Involving Sums of Products of Sparse Arrays. In *Ninth SIAM conference on Parallel Processing for Scientific Computing*.

- C.-C. Lam, P. Sadayappan, and R. Wenger. 1997. Optimal reordering and mapping of a class of nested-loops for parallel execution. In *Languages and Compilers for Parallel Computing*. Springer Berlin Heidelberg, Berlin, Heidelberg, 315–329.
- R. J. LeVeque. 2002. *Finite volume methods for hyperbolic problems*. Vol. 31. Cambridge University Press.
- J. Li, C. Battaglini, I. Perros, J. Sun, and R. Vuduc. 2015. An input-adaptive and in-place approach to dense tensor-times-matrix multiply. In *SC '15: Proceedings of the International Conference for High Performance Computing, Networking, Storage and Analysis*. 1–12.
- F. Luporini, A. L. Varbanescu, F. Rathgeber, G.-T. Bercea, J. Ramanujam, D. A. Ham, and P. H. J. Kelly. 2015. Cross-Loop Optimization of Arithmetic Intensity for Finite Element Local Assembly. *ACM Transactions on Architecture and Code Optimization* 11, 4, Article 57 (Jan. 2015), 25 pages.
- D. Matthews. 2018. High-Performance Tensor Contraction without Transposition. *SIAM Journal on Scientific Computing* 40, 1 (2018), C1–C24.
- T. Nelson, A. Rivera, P. Balaprakash, M. Hall, P. D. Hovland, E. Jessup, and B. Norris. 2015. Generating Efficient Tensor Contractions for GPUs. In *2015 44th International Conference on Parallel Processing*, 969–978.
- E. Peise and P. Bientinesi. 2012. Performance Modeling for Dense Linear Algebra. In *Proceedings of the 2012 SC Companion: High Performance Computing, Networking Storage and Analysis (SCC '12)*. IEEE Computer Society, Washington, DC, USA, 406–416.
- H. Seidl, R. Wilhelm, and S. Hack. 2012. *Compiler Design: Analysis and Transformation*. Springer.
- Y. Shi, U. N. Niranjan, A. Anandkumar, and C. Cecka. 2016. Tensor Contractions with Extended BLAS Kernels on CPU and GPU. In *2016 IEEE 23rd International Conference on High Performance Computing (HiPC)*. 193–202.
- E. Solomonik, D. Matthews, J. Hammond, and J. Demmel. 2013. Cyclops Tensor Framework: Reducing Communication and Eliminating Load Imbalance in Massively Parallel Contractions. In *2013 IEEE 27th International Symposium on Parallel and Distributed Processing*. 813–824.
- P. Springer and P. Bientinesi. 2018. Design of a High-Performance GEMM-like Tensor-Tensor Multiplication. *ACM Trans. Math. Softw.* 44, 3 (2018), 28:1–28:29.
- K. Stock, T. Henretty, I. Murugandi, P. Sadayappan, and R. Harrison. 2011. Model-Driven SIMD Code Generation for a Multi-Resolution Tensor Kernel. In *Proceedings of the 2011 IEEE Parallel and Distributed Processing Symposium*. IEEE Computer Society, 1058–1067.
- C. Uphoff and M. Bader. 2016. Generating high performance matrix kernels for earthquake simulations with viscoelastic attenuation. In *2016 International Conference on High Performance Computing and Simulation (HPCS)*. 908–916.
- C. Uphoff, S. Rettenberger, M. Bader, E. H. Madden, T. Ulrich, S. Wollherr, and A.-A. Gabriel. 2017. Extreme Scale Multi-physics Simulations of the Tsunamigenic 2004 Sumatra Megathrust Earthquake. In *Proceedings of the International Conference for High Performance Computing, Networking, Storage and Analysis (SC '17)*. ACM, New York, NY, USA, Article 21, 16 pages.
- F. G. Van Zee and R. A. van de Geijn. 2015. BLIS: A Framework for Rapidly Instantiating BLAS Functionality. *ACM Trans. Math. Software* 41, 3, Article 14 (June 2015), 33 pages.
- P. Vincent, F. Witherden, B. Vermeire, J. S. Park, and A. Iyer. 2016. Towards Green Aviation with Python at Petascale. In *Proceedings of the International Conference for High Performance Computing, Networking, Storage and Analysis (SC '16)*. IEEE Press, Piscataway, NJ, USA, Article 1, 11 pages.
- P. Wauligmann and N. W. Brei. 2019. PSpaMM: Portable Sparse Matrix Multiplication. <https://github.com/peterwauligmann/pspamm>. (2019). Accessed: 2019-01-21.
- S. Wollherr, A.-A. Gabriel, and C. Uphoff. 2018. Off-fault plasticity in three-dimensional dynamic rupture simulations using a modal Discontinuous Galerkin method on unstructured meshes: implementation, verification and application. *Geophysical Journal International* 214, 3 (2018), 1556–1584.

A SEISSOL: FULL PERFORMANCE RESULTS

Table 2. Full results of the SeisSol benchmark, where NZ:=non-zero GFLOPS and HW:=hardware GFLOPS. HW_{mad} shows the standard deviation estimated with the consistent median absolute deviation.

| Ord. | Sim. | SMT | MDoF/s | NZ _{max} | HW _{max} | HW _{mad} |
|------|------|-----|--------|-------------------|-------------------|-------------------|
| O2 | R | Yes | 770 | 134 | 1229 | 8.4 |
| O2 | 1 | Yes | 739 | 129 | 1172 | 36.8 |
| O2 | 16 | Yes | 3037 | 525 | 611 | 8.5 |
| O2 | 32 | Yes | 4034 | 697 | 808 | 12.1 |
| O3 | R | Yes | 1502 | 324 | 1709 | 5.4 |
| O3 | 1 | Yes | 1427 | 307 | 1615 | 22.6 |
| O3 | 16 | Yes | 4882 | 1038 | 1224 | 12.3 |
| O3 | 32 | No | 3857 | 820 | 962 | 10.4 |
| O4 | R | Yes | 1902 | 536 | 2122 | 56.1 |
| O4 | 1 | Yes | 1897 | 534 | 2108 | 83.2 |
| O4 | 16 | No | 4061 | 1143 | 1403 | 33.5 |
| O4 | 32 | No | 2961 | 833 | 1017 | 22.2 |
| O5 | R | Yes | 1930 | 723 | 2549 | 55.8 |
| O5 | 1 | Yes | 1949 | 730 | 2568 | 55.6 |
| O5 | 16 | Yes | 3030 | 1145 | 1469 | 33.8 |
| O5 | 32 | No | 2163 | 817 | 1043 | 89.7 |
| O6 | R | Yes | 1494 | 752 | 2902 | 5.6 |
| O6 | 1 | Yes | 1489 | 749 | 2889 | 1.4 |
| O6 | 16 | No | 2221 | 1135 | 1534 | 66.7 |
| O6 | 32 | Yes | 1603 | 818 | 1095 | 13.8 |
| O7 | R | Yes | 1204 | 806 | 2888 | 10.4 |
| O7 | 1 | Yes | 1184 | 792 | 2839 | 11.2 |
| O7 | 16 | Yes | 1191 | 814 | 1142 | 10.0 |
| O7 | 32 | Yes | 1285 | 877 | 1220 | 17.6 |

(a) KNL / SP

| Ord. | Sim. | SMT | MDoF/s | NZ _{max} | HW _{max} | HW _{mad} |
|------|------|-----|--------|-------------------|-------------------|-------------------|
| O2 | R | Yes | 687 | 120 | 548 | 12.6 |
| O2 | 1 | Yes | 670 | 117 | 531 | 11.0 |
| O2 | 8 | Yes | 2262 | 392 | 443 | 15.3 |
| O2 | 16 | Yes | 1981 | 342 | 397 | 6.8 |
| O3 | R | Yes | 1117 | 241 | 737 | 7.5 |
| O3 | 1 | Yes | 1115 | 240 | 732 | 13.7 |
| O3 | 8 | No | 2497 | 532 | 625 | 7.5 |
| O3 | 16 | No | 2295 | 488 | 573 | 29.5 |
| O4 | R | Yes | 1211 | 341 | 1154 | 14.1 |
| O4 | 1 | Yes | 1184 | 334 | 1126 | 5.7 |
| O4 | 8 | No | 2122 | 598 | 742 | 1.9 |
| O4 | 16 | Yes | 1842 | 518 | 637 | 18.6 |
| O5 | R | Yes | 1169 | 438 | 1314 | 21.4 |
| O5 | 1 | Yes | 1171 | 438 | 1314 | 14.5 |
| O5 | 8 | Yes | 1579 | 598 | 775 | 16.4 |
| O5 | 16 | No | 1370 | 518 | 664 | 16.8 |
| O6 | R | Yes | 917 | 461 | 1435 | 6.9 |
| O6 | 1 | Yes | 912 | 459 | 1426 | 9.0 |
| O6 | 8 | No | 1134 | 581 | 792 | 13.2 |
| O6 | 16 | Yes | 876 | 447 | 601 | 20.9 |
| O7 | R | No | 614 | 411 | 1343 | 79.9 |
| O7 | 1 | No | 605 | 405 | 1323 | 112.0 |
| O7 | 8 | Yes | 623 | 417 | 546 | 10.4 |
| O7 | 16 | Yes | 673 | 459 | 645 | 11.5 |

(b) KNL / DP

| Ord. | Sim. | SMT | MDoF/s | NZ _{max} | HW _{max} | HW _{mad} |
|------|------|-----|--------|-------------------|-------------------|-------------------|
| O2 | R | Yes | 510 | 89 | 815 | 3.8 |
| O2 | 1 | Yes | 530 | 92 | 840 | 0.3 |
| O2 | 16 | Yes | 2939 | 508 | 584 | 0.9 |
| O2 | 32 | Yes | 3300 | 570 | 653 | 3.9 |
| O3 | R | Yes | 1249 | 269 | 1421 | 3.5 |
| O3 | 1 | Yes | 1344 | 290 | 1521 | 10.5 |
| O3 | 16 | Yes | 3377 | 718 | 877 | 3.2 |
| O3 | 32 | Yes | 3619 | 769 | 935 | 1.6 |
| O4 | R | Yes | 1562 | 440 | 1741 | 6.0 |
| O4 | 1 | Yes | 1542 | 434 | 1714 | 26.8 |
| O4 | 16 | Yes | 3565 | 1003 | 1306 | 2.2 |
| O4 | 32 | No | 3687 | 1037 | 1343 | 0.5 |
| O5 | R | Yes | 1901 | 712 | 2511 | 21.0 |
| O5 | 1 | Yes | 1877 | 703 | 2474 | 12.4 |
| O5 | 16 | Yes | 3655 | 1382 | 1918 | 1.5 |
| O5 | 32 | Yes | 3712 | 1402 | 1937 | 20.2 |
| O6 | R | No | 1965 | 988 | 3816 | 21.7 |
| O6 | 1 | No | 1982 | 997 | 3845 | 49.8 |
| O6 | 16 | Yes | 3600 | 1840 | 2729 | 44.5 |
| O6 | 32 | Yes | 3544 | 1809 | 2660 | 58.4 |
| O7 | R | No | 1827 | 1222 | 4383 | 36.0 |
| O7 | 1 | No | 1802 | 1206 | 4321 | 42.8 |
| O7 | 16 | Yes | 3275 | 2237 | 3493 | 68.0 |
| O7 | 32 | No | 3206 | 2187 | 3389 | 8.5 |

(c) SKX / SP

| Ord. | Sim. | SMT | MDoF/s | NZ _{max} | HW _{max} | HW _{mad} |
|------|------|-----|--------|-------------------|-------------------|-------------------|
| O2 | R | Yes | 414 | 72 | 330 | 0.7 |
| O2 | 1 | Yes | 427 | 74 | 339 | 0.2 |
| O2 | 8 | Yes | 1402 | 243 | 274 | 0.2 |
| O2 | 16 | Yes | 1609 | 278 | 318 | 0.9 |
| O3 | R | Yes | 696 | 150 | 459 | 2.1 |
| O3 | 1 | Yes | 696 | 150 | 457 | 1.2 |
| O3 | 8 | Yes | 1659 | 353 | 415 | 0.6 |
| O3 | 16 | Yes | 1788 | 380 | 462 | 0.6 |
| O4 | R | Yes | 1043 | 294 | 994 | 10.3 |
| O4 | 1 | Yes | 1043 | 294 | 992 | 3.9 |
| O4 | 8 | Yes | 1770 | 499 | 619 | 0.8 |
| O4 | 16 | No | 1827 | 514 | 669 | 0.2 |
| O5 | R | Yes | 1212 | 454 | 1363 | 5.9 |
| O5 | 1 | Yes | 1199 | 449 | 1347 | 17.3 |
| O5 | 8 | No | 1807 | 684 | 887 | 2.9 |
| O5 | 16 | No | 1835 | 694 | 963 | 0.8 |
| O6 | R | Yes | 1259 | 633 | 1970 | 28.6 |
| O6 | 1 | Yes | 1244 | 626 | 1946 | 42.5 |
| O6 | 8 | No | 1784 | 914 | 1246 | 3.1 |
| O6 | 16 | No | 1766 | 902 | 1332 | 4.0 |
| O7 | R | Yes | 1048 | 702 | 2293 | 101.3 |
| O7 | 1 | Yes | 1024 | 686 | 2241 | 35.7 |
| O7 | 8 | No | 1707 | 1142 | 1495 | 27.0 |
| O7 | 16 | No | 1614 | 1103 | 1722 | 23.9 |

(d) SKX / DP